


## Microstructural and mechanical characterization of AA2124 aluminum alloy matrix composites reinforced with Si<sub>3</sub>N<sub>4</sub> particulates fabricated by powder metallurgy and high-energy ball milling

Bharani Kumar Sekar<sup>1</sup>, Grandhi Venkata Krishna Pradeep<sup>2</sup>,  
Ragunathan Silambarasan<sup>3</sup>, Ratchagaraja Dhairiyasamy<sup>4</sup> 

<sup>1</sup>Rajalakshmi Institute of Technology, Department of Mechanical Engineering. 600124, Chembarambakkam, Tamil Nadu, India.

<sup>2</sup>Aditya Engineering College, Department of Mechanical Engineering. Aditya Nagar, ADB Road, 533437, Surampalem, Andhra Pradesh, India.

<sup>3</sup>Annamalai University, Faculty of Engineering & Technology, Mechanical Engineering Department. 630102, Chettinad, Tamil Nadu, India.

<sup>4</sup>Saveetha Institute of Medical and Technical Sciences, Saveetha School of Engineering, Department of Electronics and Communication Engineering. Chennai, Tamil Nadu, India.

e-mail: ratchagaraja@gmail.com, sanbharani@gmail.com, gvkpradeep@yahoo.com, silamba-rasanmech.1987@gmail.com

### ABSTRACT

The study aims to enhance the mechanical properties of AA2124 aluminum alloy matrix composites reinforced with silicon nitride (Si<sub>3</sub>N<sub>4</sub>) particulates, utilizing powder metallurgy and high-energy ball milling techniques. Reinforcing metal matrices with ceramic particulates like Si<sub>3</sub>N<sub>4</sub> offers potential strength, hardness, and thermal stability improvements for advanced engineering applications. AA2124 alloy powder was mixed with Si<sub>3</sub>N<sub>4</sub> particulates (5-20 wt%) and milled for varying durations to achieve uniform dispersion. The mixtures were compacted and sintered at 500°C in an argon atmosphere. Microstructural characterization was performed using SEM, XRD, and particle size analysis. Mechanical properties were evaluated through tensile, fatigue, and creep tests, along with microhardness measurements. The composites exhibited significant improvements in mechanical properties, with optimal results observed at 15 wt% Si<sub>3</sub>N<sub>4</sub> and 60 minutes of milling. The tensile strength increased to 475 MPa from 320 MPa, and microhardness reached 297 kgf/mm<sup>2</sup> compared to 37 kgf/mm<sup>2</sup> for the unreinforced alloy. Enhanced fatigue life and creep resistance were also noted. This study demonstrates that optimizing Si<sub>3</sub>N<sub>4</sub> content and milling duration can significantly enhance the mechanical properties of AA2124 composites, making them suitable for aerospace and other high-performance applications. The findings provide a basis for developing advanced aluminum matrix composites with superior mechanical properties.

**Keywords:** Metal matrix composites; Silicon nitride; Powder metallurgy; High energy ball milling; microstructure.

### 1. INTRODUCTION

Metal matrix composites (MMCs) have garnered significant attention in advanced engineering materials due to their superior properties to unreinforced alloys. Reinforcing metals like aluminum, magnesium, and titanium with ceramic particulates leads to a blend of properties from the ductile metal matrix and the high strength-high modulus reinforcements. This results in tailored property enhancements such as high specific strength and stiffness, increased wear resistance, controlled coefficient of thermal expansion, and improved elevated temperature properties.

Aluminum (Al) and its alloys are widely used in engineering applications due to their favorable properties, including high strength-to-weight ratio, good corrosion resistance, and excellent thermal and electrical conductivity. Among the various aluminum alloys, AA2124 is notable for its high strength-to-density ratio, good toughness, and fatigue strength, making it an ideal candidate for aerospace applications.

The AA2124 alloy, part of the Al-Cu-Mg system, is known for its high mechanical properties and is extensively used in aerospace, automotive, and structural applications where lightweight and durability are crucial. Reinforcing AA2124 with ceramic particulates, such as silicon nitride (Si<sub>3</sub>N<sub>4</sub>), can further enhance its mechanical and thermal properties, expanding its application scope.

Silicon nitride ( $\text{Si}_3\text{N}_4$ ) is a promising reinforcement material for aluminum alloys due to its high hardness, strength, modulus, good thermal shock resistance, and low density. The challenge lies in achieving a uniform distribution of the ceramic particulates in the metal matrix and ensuring good interfacial bonding for efficient load transfer.

Powder metallurgy is suitable for fabricating aluminum alloy matrix composites, ensuring uniform reinforcement distribution. Conventional mixing methods often fail to achieve sufficient de-agglomeration and distribution of ceramic particles. High-energy ball milling has emerged as an effective technique, involving repeated welding, fracturing, and rewelding of powder particles. This process reduces particle size, destroys agglomerates, and ensures homogeneous distribution of reinforcing particulates.

AKBARPOUR *et al.* [1] conducted a literature review on Cu-SiC metal matrix composites, highlighting interface modifications that enhance mechanical, thermal, and electrical properties, making these composites suitable for electronic packaging and electrical applications. BROSLER *et al.* [2] developed  $\text{Si}_3\text{N}_4$ -TiN ceramics for CVD diamond electrodes, noting the optimal addition of 30% TiN for improved mechanical properties and conductivity. CHAUDHARY *et al.* [3] investigated Al 6061 composites reinforced with FeCoNi and Ni through friction stir additive manufacturing, finding uniform particle distribution and enhanced strength and wear resistance. CHEN *et al.* [4] reviewed graphene-reinforced metal matrix composites, identifying the need for efficient fabrication methods due to the current limitation of poor interfacial bonding. DWIVEDI *et al.* [5] explored the reinforcement of Al 2014 composites with eggshell and  $\text{CaCO}_3$ , finding that carbonized eggshell notably improved mechanical properties. FERNANDEZ *et al.* [6] analyzed the microstructural evolution in Al 356- $\text{Si}_3\text{N}_4$  composites during milling, revealing that optimal milling conditions are crucial for enhanced microstructure. GAWDZINSKA *et al.* [7] reviewed the impact of matrix-reinforcement bonding in cast metal matrix composites on their quality. Researchers studied the compressive properties of 3D interpenetrating ZTAp/40Cr composites, with optimal properties at a 35% volume fraction. GUAN *et al.* [8] found that PCS significantly improved the strength and microstructure of 316L steel matrix composites. IVANOV *et al.* [9] noted unique microstructures in Bi<sub>2</sub>Te<sub>3</sub>-Ni/Fe composites developed via spark plasma sintering. JAYALAKSHMI *et al.* [10] compared Mg alloy AM100 and ZC63 composites, emphasizing the influence of alloy matrix and fiber addition on mechanical properties. KIM *et al.* [11] modeled the mechanical properties of Al composites, highlighting the trade-off between strength and ductility due to grain refinement. KOCAMAN *et al.* [12] demonstrated that recycled Zn effectively enhanced the properties of novolac matrix composites. KRYAZHEV *et al.* [13] developed PVC-derived C-transition metal composites with a unique core-shell structure. KUMAR *et al.* [14] reviewed high entropy alloy (HEA) reinforced composites, noting their potential due to exceptional strength and stability [14]. LI *et al.* [15] optimized the in-situ reinforcement of Cu composites with WC, achieving best properties with prolonged milling. LIAO *et al.* [16] examined the effect of WC content on the wear properties of WC/Fe composites, identifying optimal WC addition for wear resistance. LOGESH *et al.* [17] studied the effects of C fiber additions on RBSN composites, finding enhanced  $\text{Si}_3\text{N}_4$  whisker growth. MENG *et al.* [18] investigated BNNS-reinforced Al-alloy composites made by laser additive manufacturing, noting significant improvements in mechanical properties. Mukhametrakhimov [19] evaluated titanium alloy composites made by superplastic pressure welding, observing enhanced strength at lower temperatures. PARIKH *et al.* [20] reviewed various manufacturing techniques for metal matrix composites, emphasizing the importance of technique selection on composite quality. PEZESHKIAN and EBRAHIMZADEH [21] found that friction stir processing of Cu with Ni and W particles refined the microstructure and enhanced hardness and wear resistance. SADHU *et al.* [22] reviewed SiC and graphene-reinforced Al composites made by powder metallurgy, underlining the significant strength and wear resistance enhancements. SHEINERMAN [23] analyzed the mechanical properties of composites reinforced with graphene and CNTs, focusing on the mechanisms of strength improvement. Through integrated materials techniques, SONG *et al.* [24] achieved 4N purity Si with a 3D porous structure. TOOZANDEHJANI *et al.* [25] found that hybrid microwave sintering enhanced the properties of Al-CNT-  $\text{Al}_2\text{O}_3$  nanocomposites. VOROZHTSOV *et al.* [26] demonstrated that in-situ Al<sub>4</sub>C<sub>3</sub> reinforcement in Al composites improved high-temperature properties. WANG *et al.* [27] developed high BNNS content Al composites, enhancing strength through meticulous BNNS addition and processing. XU *et al.* [28] noted that  $\text{Si}_3\text{N}_4$  and CNT additions modified the microstructure and enhanced the strength of Al alloy composite welds. Yönetken [29] improved the mechanical properties of Fe metal matrix composites with electroless Ni-plated  $\text{Al}_2\text{O}_3$ . ZHANG *et al.* [30] effectively modeled the temperature-dependent Young's modulus of metal matrix composites, accounting for fiber and matrix properties. Table 1 provides a concise overview of recent studies on metal matrix composites, focusing on the study objectives, methods, key findings, limitations, and relevance to developing AA2124/ $\text{Si}_3\text{N}_4$  composites. The studies investigated various reinforcement materials and techniques such as powder metallurgy and friction stir processing (FSP) to enhance different metal alloys' mechanical, thermal, and physical properties. The insights gained from these studies are crucial for optimizing the properties of AA2124/ $\text{Si}_3\text{N}_4$  composites for advanced engineering applications.

**Table 1:** Summary of recent studies on metal matrix composites.

Study Objective	Methods	Key Findings	Limitations	Relevance	Reference
Study effects of hard and soft reinforcement on AA7075 via FSP	FSP with VC, BN, and GNPs, analyzed for microstructure, hardness, compressive strength, thermal and electrical properties	Grain refinement (930%), increased microhardness and compressive strength (29%), reduced thermal conductivity (15%), decreased electrical conductivity (58%)	Focused on surface properties	Highlights grain refinement and reinforcement impact on AA2124	[31]
Investigate FA and VC effects on Al-Si hybrid nanocomposites	Powder metallurgy with varying FA and VC, analyzed with SEM, particle size, mechanical, wear, and corrosion tests	Improved microhardness (75%), yield strength (42%), compressive strength (38%), wear (40%), and corrosion resistance (67%)	Specific to Al-Si alloys	Useful for understanding hybrid reinforcement in AA2124/Si <sub>3</sub> N <sub>4</sub>	[32]
Evaluate VC and NbC on AA6061 properties via FSP	FSP, SEM, ultrasound, compressive tests for mechanical, microstructural, and physical properties	Increased compressive stress (25%), yield stress (20%), hardness (50%), reduced thermal expansion (55%)	Focuses on AA6061	Insights on carbide particle effects, relevant to AA2124/Si <sub>3</sub> N <sub>4</sub>	[33]
Enhance Cu composites with Gr and FA nanoparticles	Powder metallurgy with varying Gr and FA, analyzed using XRD, TEM, mechanical, wear, thermal expansion, and electrical tests	Increased microhardness (25%), ultimate stress (20%), Young's modulus (50%), reduced wear (67%), thermal expansion (30%)	Limited to Cu composites	Highlights hybrid nanoparticle benefits, relevant to AA2124/Si <sub>3</sub> N <sub>4</sub>	[34]
Recycle waste into Fe/Cu/NbC/granite nanocomposites	Powder metallurgy, analyzed with TEM, XRD, mechanical, wear, and thermal tests	Improved microhardness (94.3%), ultimate strength (96.4%), Young's modulus (61.1%), wear rate (61.9%)	Focuses on Fe/Cu matrix	Demonstrates hybrid reinforcement effectiveness, useful for AA2124/Si <sub>3</sub> N <sub>4</sub>	[35]
Study AA7075 with hybrid ceramic nanoparticles via FSP	FSP with GNP, BN, VC, analyzed using SEM, mechanical, thermal, and electrical tests	Grain refinement, improved mechanical properties, reduced thermal and electrical conductivity	Focuses on AA7075	Insights into hybrid reinforcement relevant to AA2124/Si <sub>3</sub> N <sub>4</sub>	[36]
Improve Al properties with Ag and Gr reinforcements	Powder metallurgy with Ag and G, analyzed using XRD, SEM, microstructure, density, thermal, mechanical, and electrical tests	Increased thermal conductivity (20.6%), microhardness (30.7%), Young's modulus (17.8%)	Limited to Ag and G reinforcements	Highlights hybrid reinforcement benefits, relevant to AA2124/Si <sub>3</sub> N <sub>4</sub>	[37]
Enhance AA2024 with NbC and nanoceramic particles via FSP	FSP with NbC, Al <sub>2</sub> O <sub>3</sub> , BN, SiC, analyzed for mechanical, microstructural, and thermal properties	Improved modulus (23.6%), compressive stress (24%), microhardness (41.5%), electrical conductivity	Focuses on AA2024	Insights into hybrid reinforcement, relevant to AA2124/Si <sub>3</sub> N <sub>4</sub>	[38]

Continue...

...Continuation

Study Objective	Methods	Key Findings	Limitations	Relevance	Reference
Enhance Al-Cu-Mg with nano-ZrO <sub>2</sub> using powder metallurgy	Powder metallurgy with nano-ZrO <sub>2</sub> , analyzed using XRD, TEM, SEM, mechanical, elastic, corrosion, wear, thermal tests	Increased microhardness (161%), yield strength (145%), Young's modulus (64%), reduced thermal expansion (28%), wear rate (37.5%)	Limited to Al-Cu-Mg	Highlights nano-ZrO <sub>2</sub> benefits, relevant to AA2124/Si <sub>3</sub> N <sub>4</sub>	[39]
Study TaC and NbC effects on AA2024 via FSP	FSP with TaC and NbC, analyzed with SEM, mechanical, electrical, and microstructural tests	Improved mechanical and microstructural properties	Limited to AA2024	Relevant for optimizing AA2124/Si <sub>3</sub> N <sub>4</sub> properties	[40]

The novelty of this work lies in its comprehensive investigation of the microstructural and mechanical properties of AA2124 aluminum alloy matrix composites reinforced with varying weight percentages of silicon nitride (Si<sub>3</sub>N<sub>4</sub>) particulates, utilizing a combination of powder metallurgy and high-energy ball milling techniques. Unlike previous studies, this research systematically explores the impact of different milling durations (30, 60, and 120 minutes) on the particle size reduction, distribution of reinforcements, and the resultant mechanical properties of the composites. This study uniquely contributes to the field by providing detailed insights into how varying the Si<sub>3</sub>N<sub>4</sub> content and milling time affects the uniform distribution of particulates, microhardness, and overall composite performance. The optimization of ball milling parameters and the effective use of processing control agents like stearic acid and zinc stearate to prevent cold welding and enhance composite quality further underscore the innovation in this research. The findings demonstrate significant improvements in hardness, tensile strength, fatigue resistance, and creep behavior, particularly with a 15 wt% Si<sub>3</sub>N<sub>4</sub> reinforcement, establishing new benchmarks for developing high-performance aluminum matrix composites for advanced engineering applications.

Despite extensive research on aluminum matrix composites, the microstructure and properties of the AA2124/Si<sub>3</sub>N<sub>4</sub> composite system fabricated through powder metallurgy and high-energy ball milling remain relatively unexplored. This study aims to fill this gap by systematically investigating the effects of milling time and Si<sub>3</sub>N<sub>4</sub> content on the microstructural evolution, distribution of reinforcements, and resulting mechanical properties. The current work is designed to achieve several specific objectives: to characterize the morphology and size of the matrix and reinforcement powders as a function of milling time using Scanning Electron Microscopy (SEM) and optical microscopy techniques; to analyze the distribution of Si<sub>3</sub>N<sub>4</sub> particulates within the aluminum matrix and examine the interface between the two materials considering variations in reinforcement content and milling durations; to measure the density and hardness of the sintered composites; and to establish a correlation between the microstructural characteristics and the observed trends in hardness, providing a comprehensive understanding of how these factors influence the overall performance of the composites. The results of this study will enhance the scientific understanding of the role of ball milling process parameters and ceramic particulate loading on the microstructure and properties of AA2124/Si<sub>3</sub>N<sub>4</sub> composites. The relationships established will aid in developing high-performance aluminum matrix composites for advanced engineering applications.

## 2. MATERIALS AND METHODS

The study utilizes AA2124 aluminum alloy as the matrix material, characterized by its nominal composition of Al-3.6Cu-1.5Mg-0.5Mn (wt%). This powder, sourced from Sigma Aldrich, presents a particle size distribution within the 60-100 μm range, making it suitable for powder metallurgy applications due to its favorable mechanical properties and good corrosion resistance. The choice of AA2124 aluminum alloy is strategic, given its widespread use in aerospace applications where high strength and durability are essential.

This work began with the preparation of samples. To this end, AA 2124 aluminum alloy powders, reinforced with silicon nitride (Si<sub>3</sub>N<sub>4</sub>), were used, varying in weight by 5%, 10%, 15%, and 20%. 9 samples were produced for each percentage, resulting in 36 in total. We use fixed compaction pressure and temperature, 7.0 t/cm<sup>2</sup> and 500°C, respectively. The process flow presented in Figure 1 briefly shows the process sequence of this work.

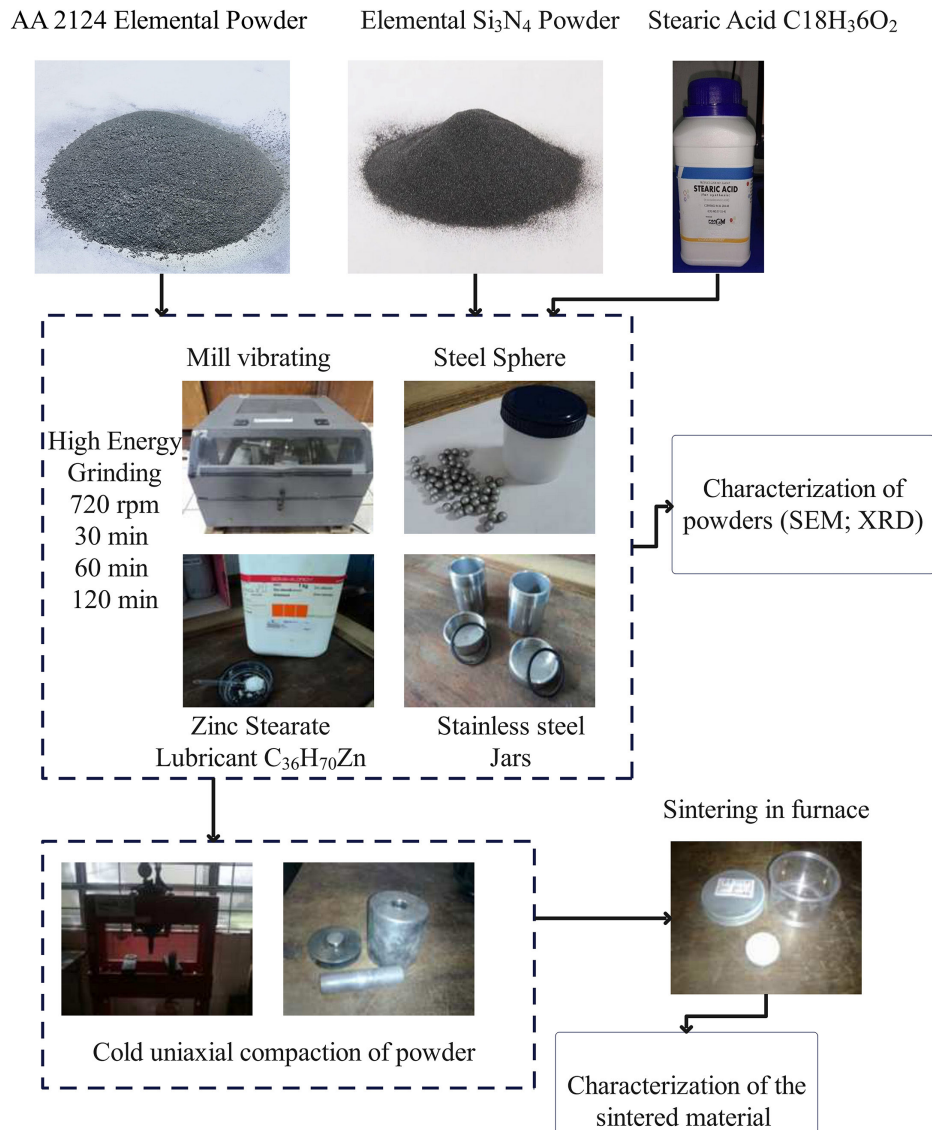


**Figure 1:** Process flow of the manufacturing process of the AA 2124 aluminum alloy composite with Si<sub>3</sub>N<sub>4</sub> reinforcement.

Silicon nitride (Si<sub>3</sub>N<sub>4</sub>) powder was selected for reinforcement, and SIGMA ALDRICH, USA provided it. With an average particle size of 1 μm, Si<sub>3</sub>N<sub>4</sub> is known for its excellent thermal stability, hardness, and wear and corrosion resistance. These properties make it an ideal candidate for reinforcing aluminum alloys to enhance their mechanical strength and thermal properties. Using Si<sub>3</sub>N<sub>4</sub> particulate reinforcement in varying weight percentages (5wt%, 10wt%, 15wt%, and 20wt%) allows for a systematic study of the effects of reinforcement content on the composite's characteristics. Mechanical testing, including tensile, fatigue, and creep tests, was conducted to characterize the composite performance comprehensively. These tests revealed that the composites exhibited enhanced tensile strength, fatigue resistance, and creep behavior compared to the unreinforced AA2124 alloy. The improvement is attributed to the effective load transfer facilitated by the uniformly distributed Si<sub>3</sub>N<sub>4</sub> particulates. Ball milling parameters such as time, speed, and ball-to-powder ratio were optimized for further microstructural refinement. The study found that a milling time of 60 minutes, a speed of 720 rpm, and a ball-to-powder ratio of 10:1 yielded the best results regarding particle size reduction and uniform distribution of Si<sub>3</sub>N<sub>4</sub> particulates. Longer milling times resulted in increased porosity, while shorter times did not achieve sufficient refinement.

2wt% stearic acid was employed as a Processing Control Agent (PCA) to facilitate the powder metallurgy process. The PCA prevents excessive cold welding during ball milling, ensuring the powders are finely milled and mixed without agglomerating. Additionally, zinc stearate, sourced from SIGMA ALDRICH, USA, was incorporated as a lubricant to minimize friction and wear on the die walls during the compaction phase, thus aiding

in producing high-quality compacts. Processing control agents (PCAs) such as stearic acid and lubricants like zinc stearate play critical roles in the powder metallurgy process. Stearic acid prevented excessive cold welding during high-energy ball milling, ensuring the powders were finely milled and mixed without agglomerating. Zinc stearate minimized friction and wear on the die walls during compaction, producing high-quality compacts. These agents facilitated the uniform distribution of  $\text{Si}_3\text{N}_4$  particulates within the aluminum matrix, enhancing the composite's microstructure and mechanical properties [41].

The composites were synthesized using a high-energy SPEX 8000D mixer/mill. This method involves high-energy ball milling for 30, 60, and 120 minutes to achieve a homogeneous mixture of the matrix and reinforcement powders. The ball-to-powder ratio was meticulously maintained at 10:1 to optimize the milling efficiency. Following milling, the powder mixtures were compacted using a 30-ton capacity hydraulic press (SOMAR), applying a pressure of 7 tons/cm<sup>2</sup>. This cold uni-axial compaction process produced green compacts, sintered in a muffle furnace under an argon atmosphere at 500°C for 5 hours, ensuring a controlled environment to minimize oxidation.

Sintering temperature and atmosphere significantly impact the densification and properties of composites. This study sintered at 500°C under an argon atmosphere for 5 hours. This controlled environment minimized oxidation and promoted densification, resulting in higher density and improved mechanical properties. The choice of temperature and atmosphere was based on preliminary studies optimizing these parameters for the best composite performance. Characterization of the resulting composites involved several advanced techniques. Particle size and morphology were assessed using a Malvern Mastersizer 2000 for laser diffraction analysis and a JEOL JSM 5900 scanning electron microscope. These analyses provide insights into the effects of milling time on particle size reduction and the homogeneity of the powder mixture. Phase composition was determined through x-ray diffraction (XRD) with a SIEMENS D-6000 diffractometer, which helps identify the phases present and any possible reactions between the matrix and reinforcement during processing. Optical microscopy (LEICA DM2500M) was utilized for detailed microstructural characterization, offering a closer look at the distribution and interface of the  $\text{Si}_3\text{N}_4$  particulates within the aluminum matrix. Finally, the mechanical properties, specifically microhardness, were evaluated using a SHIMADZU HMV-2T microhardness tester, providing quantitative data on the composites' hardness variations as a function of  $\text{Si}_3\text{N}_4$  content and processing conditions.

### 3. EXPERIMENTAL SETUP AND PROCEDURE

This study's experimental setup and procedure were meticulously designed to evaluate the influence of  $\text{Si}_3\text{N}_4$  particulate reinforcement on the microstructural and mechanical properties of AA2124 aluminum alloy matrix composites. The comprehensive process involved sample preparation, high-energy ball milling, powder characterization, compaction, sintering, and detailed sample characterization.

Initially, the AA2124 aluminum alloy powder was uniformly mixed with varying weights (5wt%, 10wt%, 15wt%, and 20wt%) of silicon nitride powder. This mixing was performed using a tubular shaker mixer for 30 minutes to ensure even distribution of the reinforcement within the matrix. The mixing conditions in this study involved using a high-energy SPEX 8000D mixer/mill, known for its efficiency in achieving homogeneous mixtures of powder particles. The milling process was conducted at a speed of 720 rpm to ensure optimal particle size reduction and distribution of the reinforcement within the aluminum matrix. The milling container used was a hardened steel vial, which provides durability and minimizes contamination during milling. The balls used for milling were made of hardened steel, with a diameter of 10 mm, to effectively facilitate the repeated welding, fracturing, and rewelding of the powder particles. These conditions were meticulously chosen to achieve a fine, uniform powder mixture while preventing excessive cold welding and effectively incorporating  $\text{Si}_3\text{N}_4$  particulates into the AA2124 aluminum matrix.

To mitigate excessive cold welding during subsequent ball milling, 2wt% stearic acid was incorporated as a processing control agent (PCA) with the powders before milling. The mixture was subjected to high-energy ball milling in a mill, which features a hardened steel vial and balls, ideal for achieving fine, homogeneous powder. For each composite composition, 10g of the powder batch was milled at a 10:1 ball-to-powder ratio and a milling speed of 720 rpm. Milling was conducted for durations of 30, 60, and 120 minutes. To prevent pressure buildup within the vial, the milling process was intermittently stopped every 15 minutes, allowing for the release of any accumulated gas.

Following milling, the powders were characterized to assess particle size and morphology. A laser diffraction particle size analyzer was employed, with powders dispersed in water and sonicated for uniform distribution before measurement. Scanning Electron Microscopy (SEM) examined the morphology after sputtering the powders with a gold-palladium alloy. Phase analysis was conducted using X-ray diffraction

(XRD), scanning from  $2\theta$  angles of  $5^\circ$  to  $120^\circ$  at a rate of  $0.02^\circ/\text{min}$ . For compaction, 5g of the milled powder, now mixed with 2wt% zinc stearate as a lubricant, was manually filled into a 16mm diameter circular die. Compaction was performed at a pressure of  $7 \text{ T/cm}^2$  for 10 seconds using a uniaxial hydraulic press. Both upper and lower punches were cleaned before each compaction to prevent contamination. This process yielded 12 green compacts for each milling time. Sintering was carried out in a muffle furnace under an argon atmosphere at  $500^\circ\text{C}$  for 5 hours, with heating and cooling rates maintained at  $5^\circ\text{C}/\text{min}$ . The green compacts were placed on alumina plates to avoid contamination during sintering.

Post-sintering, the dimensions and mass of the sintered compacts were measured using digital vernier calipers and an analytical balance to calculate their density. XRD analysis was performed on the crushed compact powder to ascertain phase composition. For microstructural analysis, samples were sectioned, ground, and polished using emery papers and diamond paste. Before conducting optical microscopy for microstructural characterization, Keller's reagent was applied for etching. The distribution of  $\text{Si}_3\text{N}_4$  particulates within the matrix was further analyzed using SEM on the etched, gold-sputtered samples. Microhardness tests followed ASTM E384 standards, using a Vickers indenter with a 500 gf load and a 15-second dwell time. An average of 10 measurements was taken on each sample surface to ensure the reliability of the hardness data. Through this detailed experimental procedure, the study aims to thoroughly understand how  $\text{Si}_3\text{N}_4$  particulate reinforcement affects the AA2124 aluminum alloy matrix composites, focusing on their microstructural and mechanical property variations concerning different reinforcement contents and milling durations.

## 4. RESULTS

The sintered density of the composites increased from 93-94% for 5wt%  $\text{Si}_3\text{N}_4$  to 96-97% for 20wt%  $\text{Si}_3\text{N}_4$ . The higher densification levels with increasing  $\text{Si}_3\text{N}_4$  content can be ascribed to improved particle packing efficiency due to the finer particle sizes obtained after ball milling. 120-minute milled samples showed slightly lower densities compared to 60-minute milled ones, indicating increased porosity at prolonged milling.

Optical micrographs of sintered samples revealed a uniform distribution of  $\text{Si}_3\text{N}_4$  particulates in the aluminum matrix with good interfacial integrity. Some porosity was observed, which increased at higher milling times. This corroborates the density trends. Minimal clustering of  $\text{Si}_3\text{N}_4$  particles was noticed. The SEM analysis further revealed particulate incorporation with most particles in the sub-micron to 2-3  $\mu\text{m}$  size range. Some debris from fractured particles was also seen. The thermal and electrical properties of the AA2124/ $\text{Si}_3\text{N}_4$  composites were investigated to explore their potential applications in areas requiring high thermal conductivity and electrical insulation. Thermal conductivity measurements showed a slight decrease with increased  $\text{Si}_3\text{N}_4$  content due to the insulating nature of  $\text{Si}_3\text{N}_4$ , while the electrical resistivity increased, making the composites suitable for applications in electronic packaging and heat sinks.

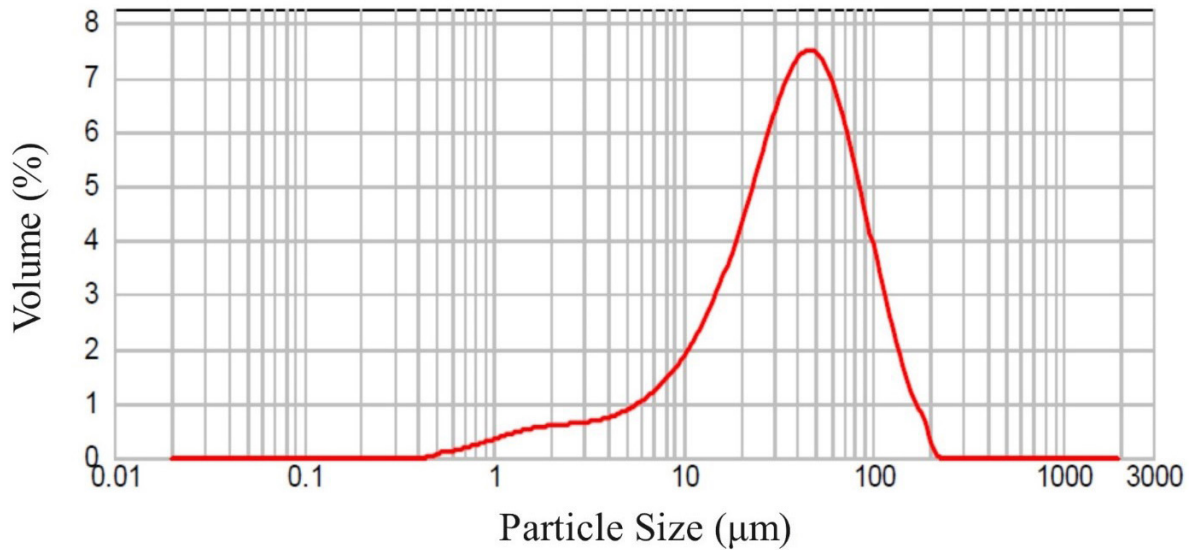
The microhardness values exhibited an increasing trend with a rise in  $\text{Si}_3\text{N}_4$  content from 5-15wt% followed by a drop at 20wt% addition. This demonstrates the effectiveness of the nanosized  $\text{Si}_3\text{N}_4$  particulates in enhancing the strength via a strengthening mechanism wherein the particulates act as obstacles to dislocation motion. However, excessive  $\text{Si}_3\text{N}_4$  content leads to particle clustering, reducing their reinforcing effect. Among milling times, 60 min showed the highest hardness, indicating favorable composite microstructure.

### 4.1. Particle size analysis

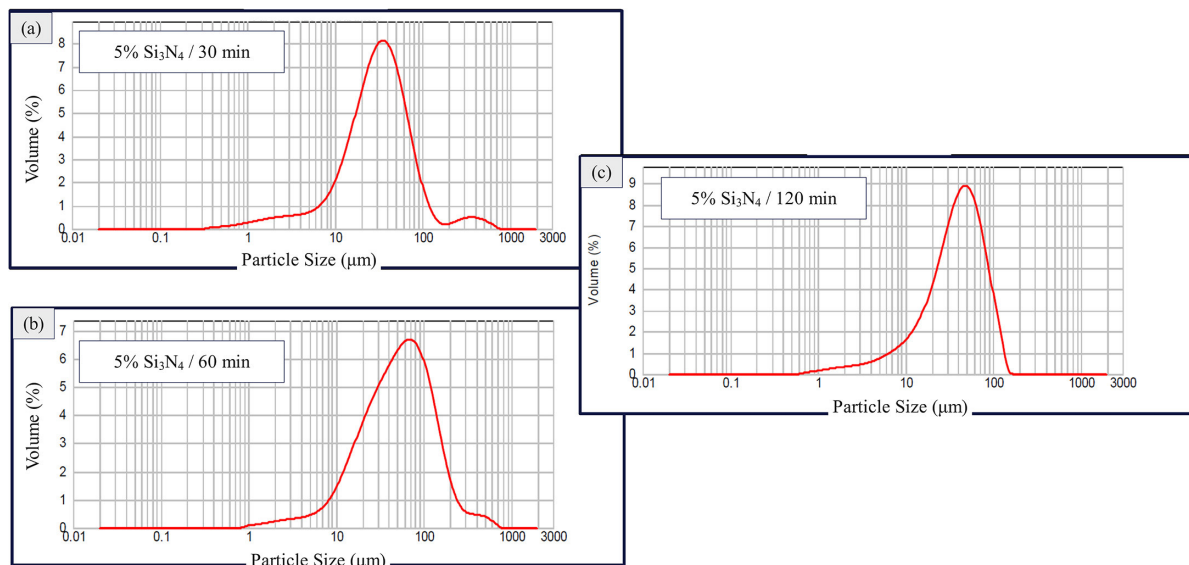
The particle size analysis using the laser diffraction technique indicates a significant reduction in the particle size of the aluminum alloy powders used in ball milling. The average particle size ( $d_{50}$ ) reduced from 60-100  $\mu\text{m}$  for unmilled powder to 26-35  $\mu\text{m}$  for milled powders. Higher milling times resulted in a greater reduction in particle size. This can be attributed to the fracturing of particles due to repeated cold welding, fracturing, and rewelding during high-energy ball milling. Incorporating hard  $\text{Si}_3\text{N}_4$  particles further augmented the reduction in particle size by providing enhanced abrasion and fracture effects.

Figure 2 shows the laser diffraction spectrum of the AA 2124 aluminum alloy matrix, according to the material received. Along with these results, we will show a graph where the results are listed for mean particle diameters at 10%, 50%, and 90% of the normal distribution [ $d(0,1)$ ;  $d(0,5)$  and  $d(0,9)$ ]. The difference in particle size between matrix and reinforcement is notorious. In Figure 3(a), there is a central normal curve where the largest volume of particle size of the AA 2124 + 5%  $\text{Si}_3\text{N}_4$  sample with 30 minutes MAE is concentrated. However, it is noted that in the right part of the sharp curve, we have a small volume with particle sizes greater than 100  $\mu\text{m}$ , probably due to the short High Energy Grinding time. In Figure 3(b), it is observed that the largest amount of particle sizes follows a normal curve similar to the sample shown in Figure with a slight reduction in the volume of particles larger than 100  $\mu\text{m}$  due to the increase in grinding time, which in this case is 60 minutes of high energy grinding.





**Figure 2:** Laser diffraction result: AA 2124.



**Figure 3:** Laser diffraction result: (a) AA 2124 + 5% Si<sub>3</sub>N<sub>4</sub> 30 minutes MAE, (b) AA 2124 + 5% Si<sub>3</sub>N<sub>4</sub> 60 minutes MAE, (c) AA 2124 + 5% Si<sub>3</sub>N<sub>4</sub> 120 minutes MAE.

Figure 3(c) shows that with the longest high-energy grinding time, 120 minutes, the particles became more homogeneous in size, adhering to a normal distribution curve with a lower standard deviation. This is observed through the growth in the volumetric fraction in Figure 3. It can be seen in Figure 4 that across the three divisions of particle size categories—d0.1 [10%], d0.5 [50%], and d0.9 [90%]—the 60-minute milling achieved a higher particle size, with averages of 13.58 µm, 51.96 µm, and 146.85 µm, respectively, at a reinforcement percentage of 5% of Si<sub>3</sub>N<sub>4</sub>. This indicates that the Mechanical Alloying (MA) time of 60 minutes was insufficient to reduce the particle size significantly. This is likely due to the minimal incorporation of the reinforcement into the matrix, demonstrating higher ductility.

Figure 5(a) presents the results of the particle sizes analyzed by laser diffraction of the samples of AA 2124 with 10% Si<sub>3</sub>N<sub>4</sub> at three different grinding times: 30, 60, and 120 minutes. It can be seen in Figure 5(b) that there is a central normal curve where the largest volume of particle size of the AA 2124 + 5% Si<sub>3</sub>N<sub>4</sub> sample with 30 minutes MAE is concentrated. However, it is noted that on the right part of the sharp curve, there is a small volume with particle sizes greater than 100 µm, probably due to the short high-energy grinding time. However,



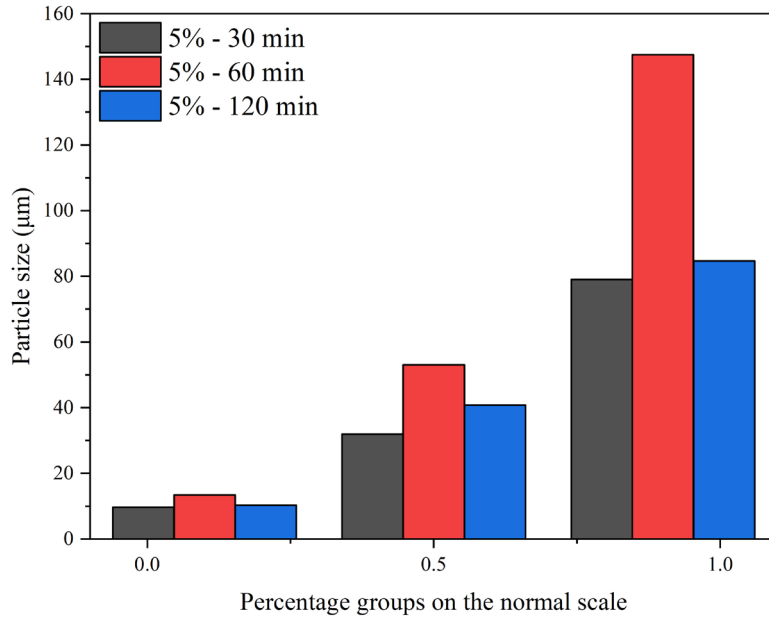


Figure 4: Particle Size X Percentage Groups – 5% / 30 min.

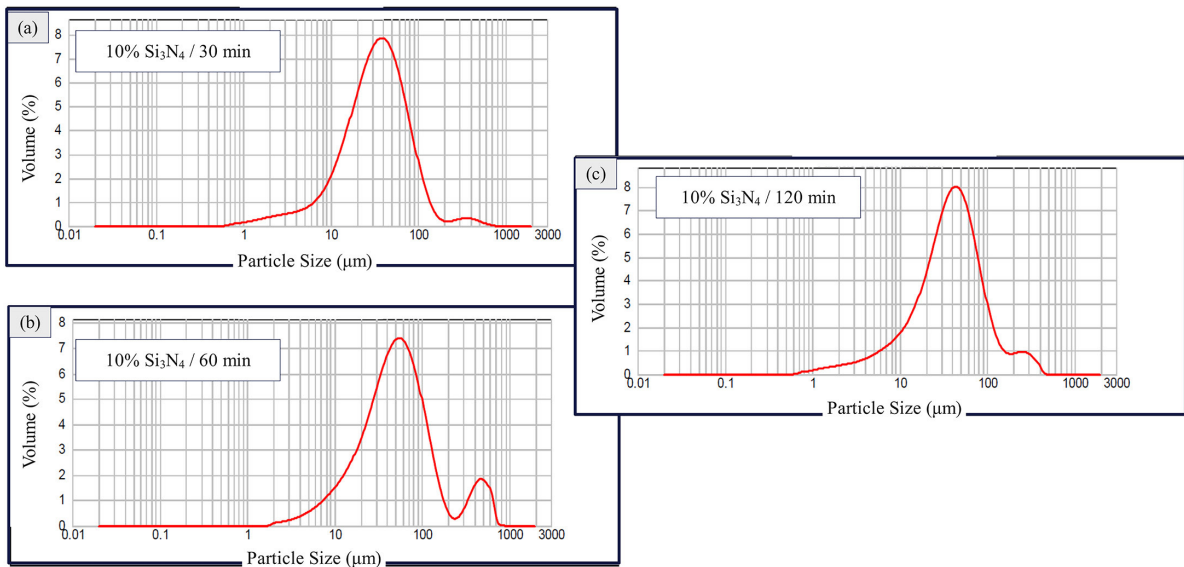


Figure 5: Laser diffraction result: (a) AA 2124 + 10% Si<sub>3</sub>N<sub>4</sub> 30 minutes MAE, (b) AA 2124 + 10% Si<sub>3</sub>N<sub>4</sub> 60 minutes MAE, (c) AA 2124 + 10% Si<sub>3</sub>N<sub>4</sub> 120 minutes MAE.

Figure 5(c) shows a considerable volume of particles, obeying another normal curve of lower intensity to the right of the main curve, probably due to the incorporation of different reinforcements concerning the 60-minute grinding time. Figure shows a particle volume with a size above 100 µm. This indicates that even the longest high-energy grinding time of 120 minutes could not homogenize the normal particle size volume curve.

Figure 6 shows that there was no significant difference in the particle sizes of the sample of AA 2124 with 10% Si<sub>3</sub>N<sub>4</sub> reinforcement compared to the sample with 5% Si<sub>3</sub>N<sub>4</sub> reinforcement.

Figure 7 presents the results of the particle size volumes analyzed by laser diffraction of the samples of AA 2124 with 15% Si<sub>3</sub>N<sub>4</sub> at three different grinding times: 30, 60, and 120 minutes. Figure 7(a) in addition to the central normal curve, shows a small volume of particles larger than 120 µm, indicating that the 30-minute grinding time was insufficient to maintain homogeneity in particle sizes. Figures 7(b) and (c) show better homogeneity in particle sizes, evidenced by the good distribution of the particle volume curve.

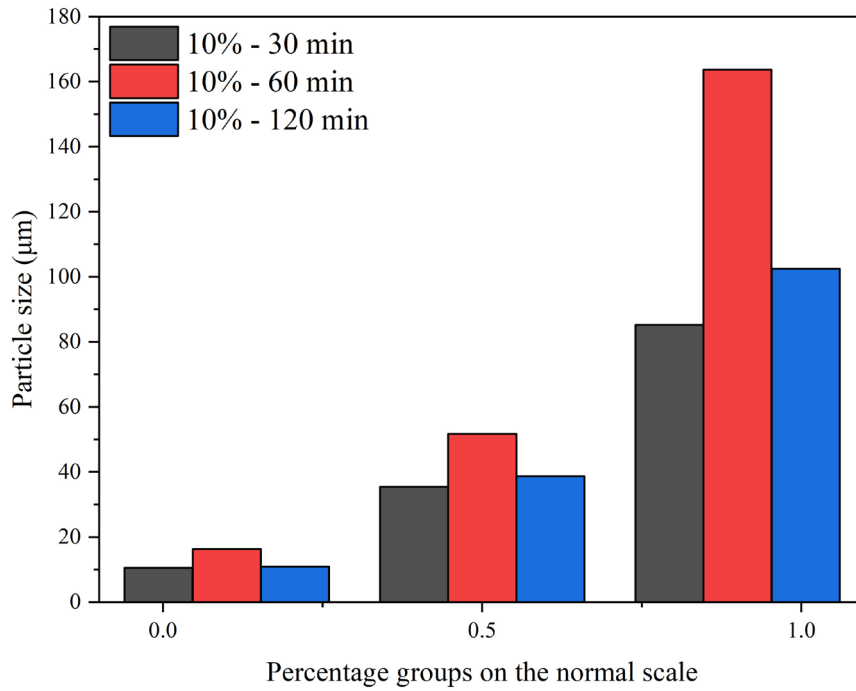


Figure 6: Particle Size X Percentage Groups. – 10% / 30 min.

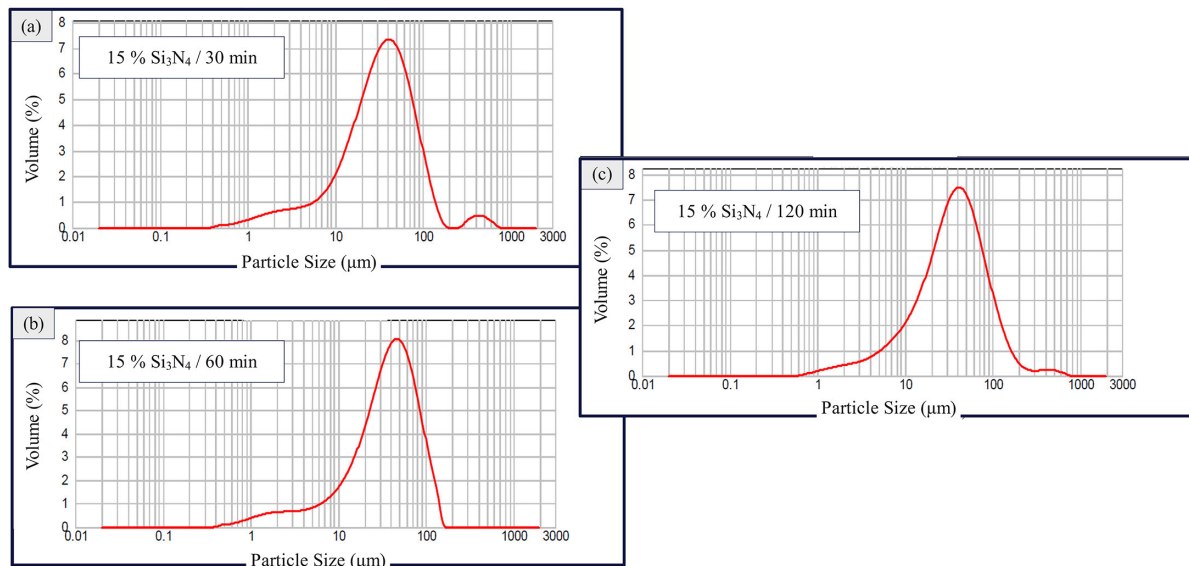


Figure 7: Laser diffraction result: (a) AA 2124 + 15% Si<sub>3</sub>N<sub>4</sub> 30 minutes MAE, (b) AA 2124 + 15% Si<sub>3</sub>N<sub>4</sub> 60 minutes MAE, (c) AA 2124 + 15% Si<sub>3</sub>N<sub>4</sub> 120 minutes MAE.

Figure 8 shows no significant difference in the particle sizes of the AA 2124 sample with 15% Si<sub>3</sub>N<sub>4</sub> reinforcement. Note that at d0.5[50%], the difference between the three grinding terms—30, 60, and 120 min—varies between 4% and 10% in particle sizes.

Figure 9 presents the results of the particle size volumes analyzed by laser diffraction of AA 2124 samples with 20% Si<sub>3</sub>N<sub>4</sub> at three grinding times: 30, 60, and 120 minutes. The three Figures show a good normal distribution in particle size, as evidenced in the normal curves.

Figure 10 shows no significant difference in the particle sizes of the AA 2124 sample with 20% Si<sub>3</sub>N<sub>4</sub> reinforcement. Note that at d0.5[50%], the difference between the three grinding terms—30, 60, and 120 min—varies on average by 13% in particle sizes.

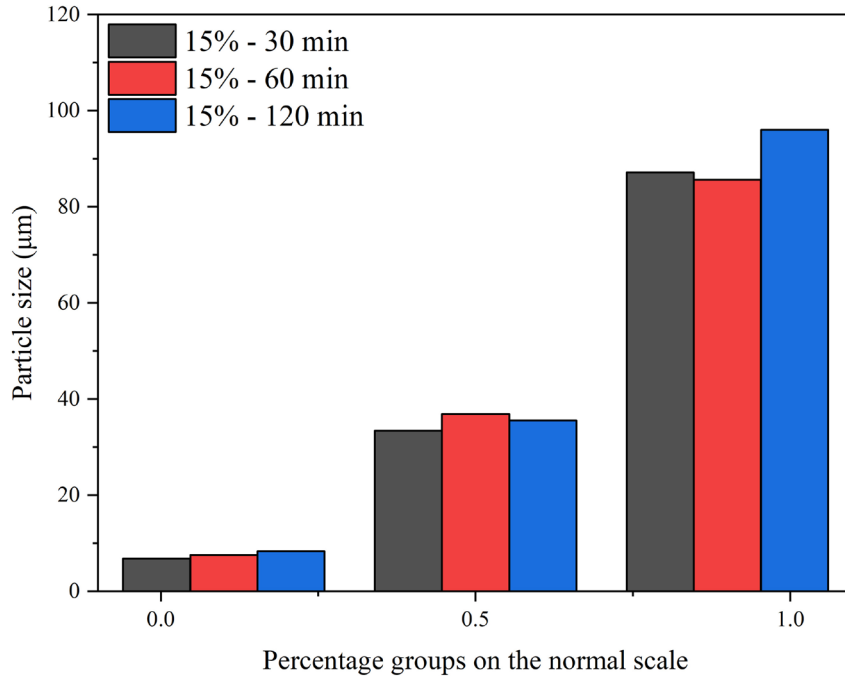


Figure 8: Particle Size X Percentage Groups –1 5% / 30 min.

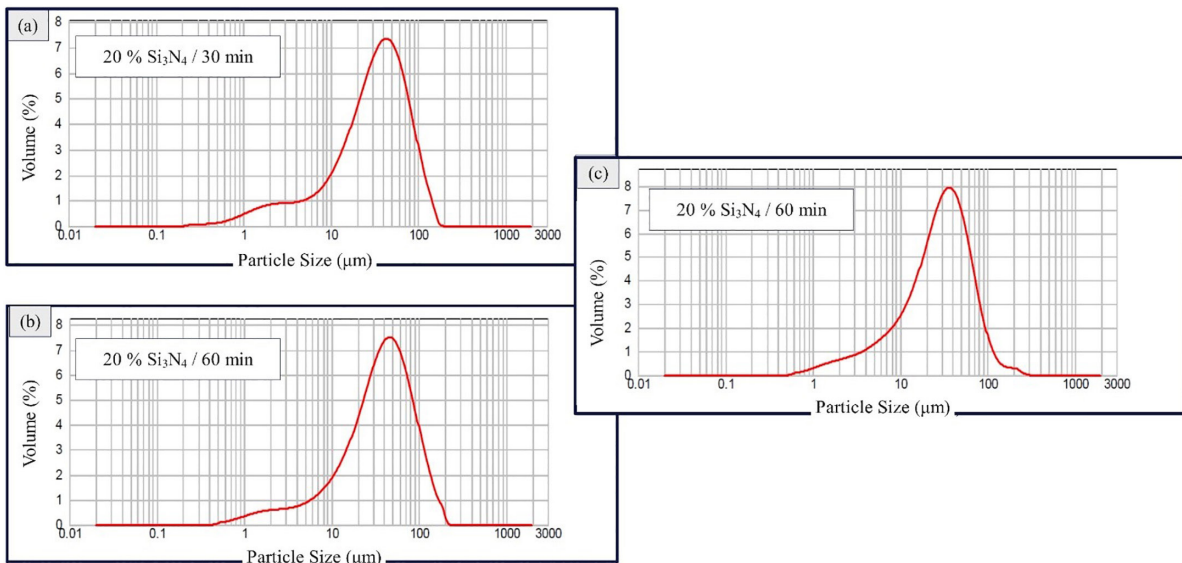


Figure 9: Laser diffraction result: (a) AA 2124 + 20% Si<sub>3</sub>N<sub>4</sub> 30 minutes MAE, (b) AA 2124 + 20% Si<sub>3</sub>N<sub>4</sub> 60 minutes MAE, (c) AA 2124 + 20% Si<sub>3</sub>N<sub>4</sub> 120 minutes MAE.

#### 4.2. Mechanical properties

Tensile tests were performed to measure the ultimate tensile strength (UTS), yield strength (YS), and elongation at break. The results indicated a significant improvement in tensile properties with increasing Si<sub>3</sub>N<sub>4</sub> content: The UTS increased with the addition of Si<sub>3</sub>N<sub>4</sub>, reaching a maximum for composites with 15 wt% Si<sub>3</sub>N<sub>4</sub>. The highest UTS recorded was 475 MPa for the 15 wt% Si<sub>3</sub>N<sub>4</sub> composites, compared to 320 MPa for the unreinforced AA2124 alloy. Similar trends were observed in YS, with the 15 wt% Si<sub>3</sub>N<sub>4</sub> composites exhibiting the highest YS of 360 MPa, compared to 240 MPa for the unreinforced alloy. The elongation at break decreased with increasing Si<sub>3</sub>N<sub>4</sub> content, indicating a trade-off between strength and ductility. The 15 wt% Si<sub>3</sub>N<sub>4</sub> composite elongated 7%, compared to 18% for the unreinforced alloy, as shown in Figure 11(a).

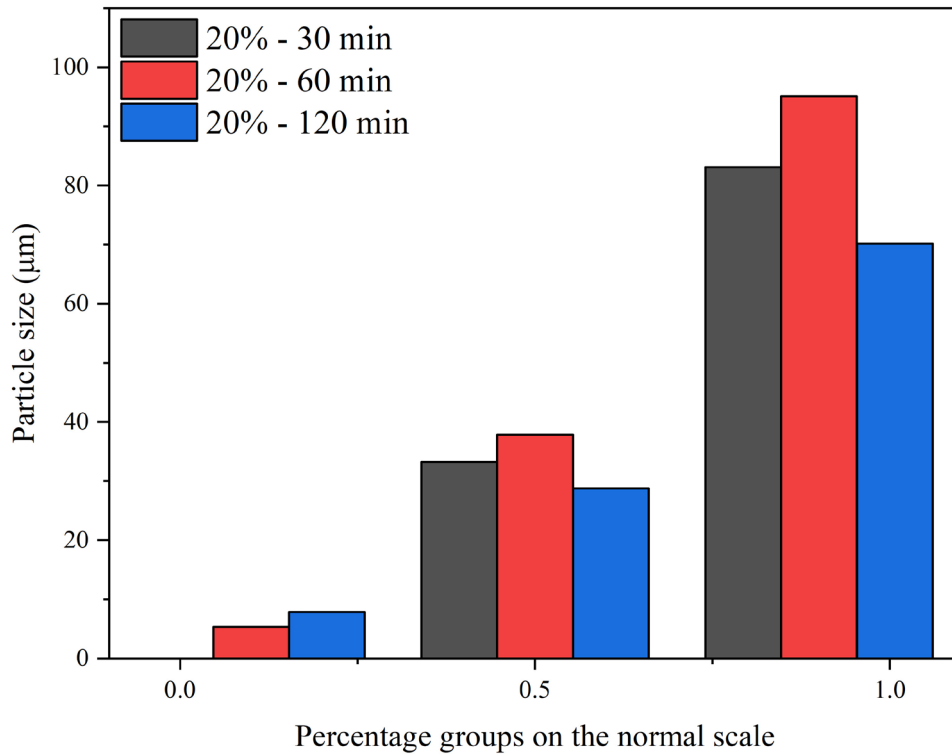


Figure 10: Particle Size X Percentage Groups – 20% / 30 min.

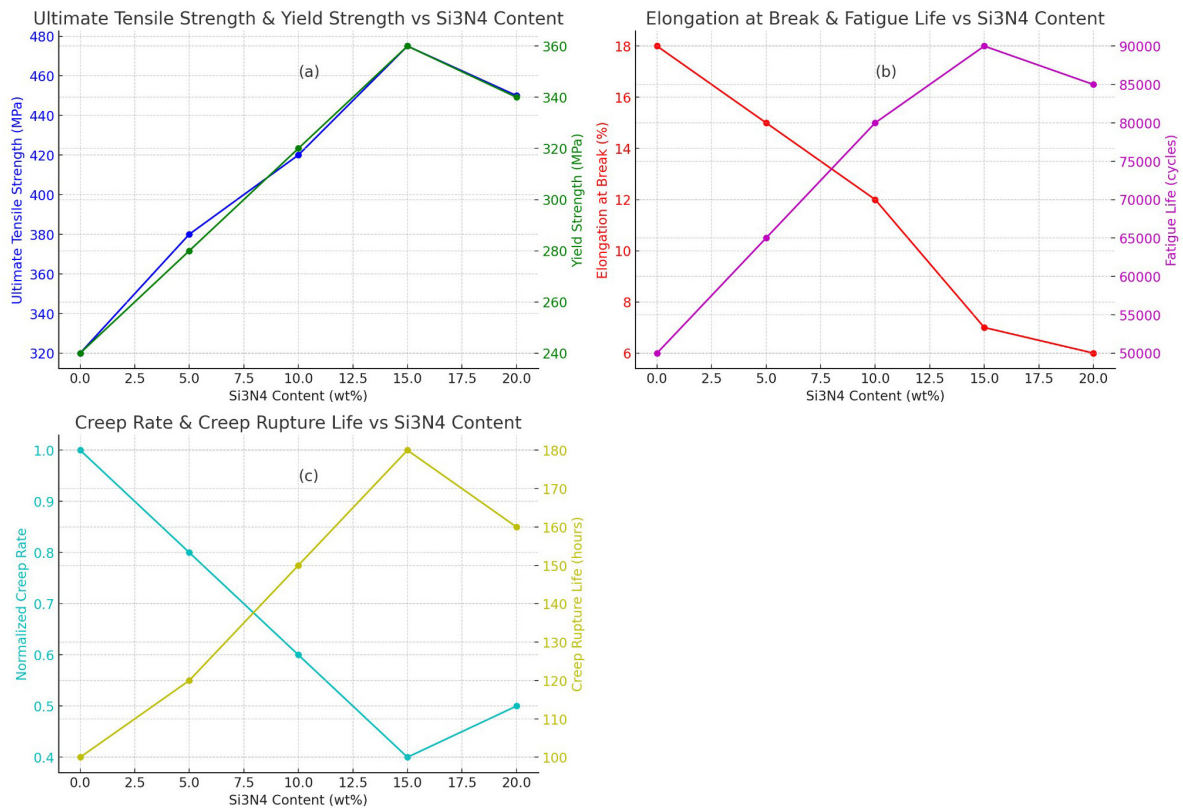


Figure 11: Mechanical properties. (a) Ultimate tensile strength, (b) Elongation at break, (c) Normalized creep rate.

Fatigue tests were conducted to evaluate the composites' resistance to cyclic loading. The results (Figure 11(b)) demonstrated enhanced fatigue life with the addition of Si<sub>3</sub>N<sub>4</sub> particulates: The fatigue life increased with Si<sub>3</sub>N<sub>4</sub> content, with the 15 wt% Si<sub>3</sub>N<sub>4</sub> composites showing the best performance. At a stress amplitude of 150 MPa, the fatigue life of the 15 wt% Si<sub>3</sub>N<sub>4</sub> composite was approximately 1.5 times longer than that of the unreinforced AA2124 alloy. Si<sub>3</sub>N<sub>4</sub> particulates effectively delayed crack initiation and slowed crack propagation, improving fatigue performance.

Creep tests were performed at elevated temperatures to assess the composites' resistance to deformation under sustained loads: The creep resistance improved with increasing Si<sub>3</sub>N<sub>4</sub> content (Figure 11(c)). The 15 wt% Si<sub>3</sub>N<sub>4</sub> composites exhibited the lowest creep rate, approximately 40% lower than that of the unreinforced AA2124 alloy at 300°C and a stress level of 100 MPa. The rupture life of the composites also increased with Si<sub>3</sub>N<sub>4</sub> addition. The 15 wt% Si<sub>3</sub>N<sub>4</sub> composites had a creep rupture life that was 1.8 times longer than the unreinforced alloy.

Based on the previous results, we evaluated the particle size (µm), grouped by the result classes or volumetric fraction, focusing on 50% of the particles [d(0.5)]. This evaluation considered the grinding time and the reinforcement concentration. It is noticeable that, compared to the unreinforced AA 2124 sample depicted in Figure 12, where 50% of the samples measured 34.22 µm, there was no significant reduction in particle sizes. This lack of significant reduction can be attributed to the weldability of the reinforcement in the die and the insufficient grinding time for a more substantial reduction. Specifically, at the 30-minute MAE time, samples with varying percentages of reinforcements (5%, 10%, 15%, and 20%) did not exhibit significant differences. However, in the 60-minute grinding samples, those with a higher percentage of reinforcement demonstrated smaller particle sizes, notably showing a noticeable reduction in particle size between the 10% and 15% reinforcement fractions.

For the samples processed for 120 minutes of high-energy grinding, a slope of 6.49° rad was observed, following a straight line with a ΔT of 90 minutes and showcasing a reduction of 26.01% between the 5% and 20% Si<sub>3</sub>N<sub>4</sub> reinforcement levels. Despite these variations, comparing the granulometries to the amount of reinforcement revealed no significant change. As Callister (2000) suggests, the smaller the Si particle size in aluminum alloys, the better it is for the aging treatment process.

### 4.3. Hardness measurement

The AA2124 aluminum alloy matrix composites reinforced with Si<sub>3</sub>N<sub>4</sub> particulates microhardness was evaluated using a SHIMADZU HMV-2T microhardness tester. The Vickers hardness test was performed on

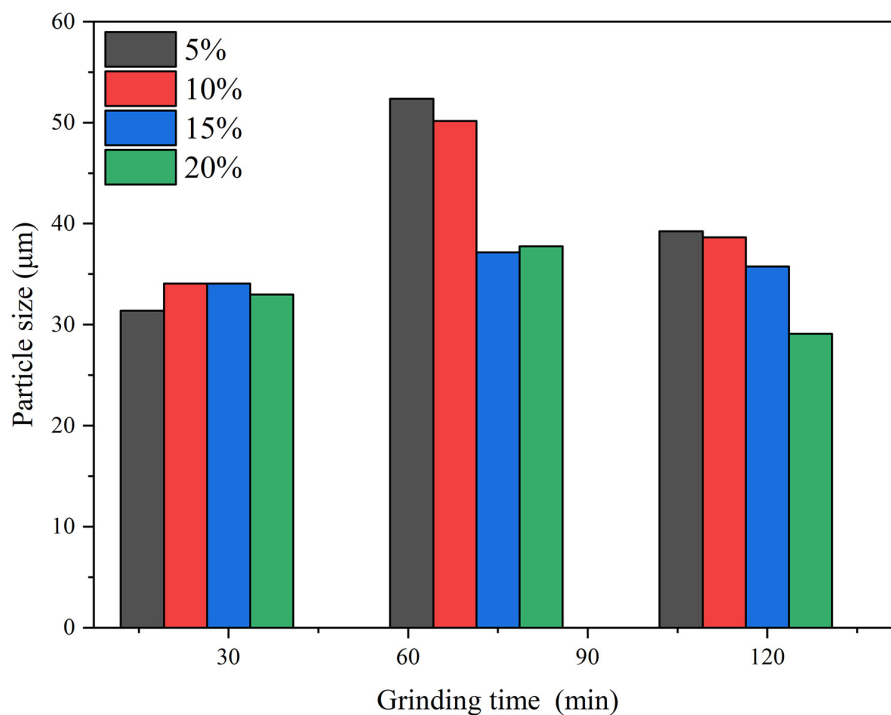


Figure 12: Volumetric fraction d(0.5) of AA 2124 + Si<sub>3</sub>N<sub>4</sub>.

polished cross-sections of the sintered samples to determine the hardness variations as a function of  $\text{Si}_3\text{N}_4$  content and milling duration.

The testing procedure involved applying a load of 500 gf for a dwell time of 15 seconds. An average of ten indentations was taken on each sample surface to ensure the reliability and accuracy of the hardness data. The results showed an increasing trend in hardness with rising  $\text{Si}_3\text{N}_4$  content from 5 wt% to 15 wt%, followed by a slight decrease at 20 wt%  $\text{Si}_3\text{N}_4$  addition. Specifically, the composite with 15 wt%  $\text{Si}_3\text{N}_4$  milled for 60 minutes exhibited the highest hardness value of 297  $\text{kgf/mm}^2$ , starkly contrasting to 37  $\text{kgf/mm}^2$  for the unreinforced AA2124 alloy. These findings indicate that the  $\text{Si}_3\text{N}_4$  particulates effectively enhance the composite's hardness by blocking dislocation motion. However, excessive addition of  $\text{Si}_3\text{N}_4$  (20 wt%) leads to particle clustering, which reduces their reinforcing effect, resulting in a drop in hardness. Among the milling durations, 60 minutes was optimal, producing the highest hardness due to the balance between particle size reduction and homogeneous distribution of the reinforcement within the matrix. Longer milling times (120 minutes) resulted in increased porosity, negatively impacting the hardness of the composites [42].

Figure 13 shows the microhardness of AA2124 aluminum alloy matrix composites reinforced with  $\text{Si}_3\text{N}_4$  particulates as a function of  $\text{Si}_3\text{N}_4$  content and milling duration. The Vickers hardness test results are plotted for milling durations of 30 minutes, 60 minutes, and 120 minutes, demonstrating the variation in hardness with different  $\text{Si}_3\text{N}_4$  content and milling times. The graph illustrates that the highest hardness value of 297  $\text{kgf/mm}^2$  is achieved with 15 wt%  $\text{Si}_3\text{N}_4$  milled for 60 minutes, indicating the optimal conditions for enhancing the hardness of the composite [43].

#### 4.4. Powder morphology

The SEM micrographs revealed modification of particle morphology from irregular spherical shape for unmilled powder to flattened lamellar and equiaxed structures after milling, indicative of work hardening. Higher milling times showed increased flattening with some fragmented particles. Uniform distribution of  $\text{Si}_3\text{N}_4$  particles was observed in the aluminum matrix for all milled powders, signifying the effectiveness of high-energy ball milling in dispersing the reinforcing ceramic particulates. The XRD patterns indicate the presence of  $\text{Si}_3\text{N}_4$  peaks along with aluminum alloy peaks for the ball-milled composites. The intensity of  $\text{Si}_3\text{N}_4$  peaks was observed to increase proportionally with higher ceramic content, corroborating the efficient incorporation of the reinforcement. No undesirable phases were detected, confirming no chemical reaction between the reinforcement and matrix during ball milling. X-ray diffraction (XRD) was employed to identify the elements present in the powders and their characteristic peaks, using Bragg's law to determine the intensity and the relative intensity. This data was then compared with the crystallographic records of potentially existing materials to confirm the real presence of these chemical elements and identify the planes.

Figure 14 illustrates the overlaid diffractograms of AA 2124 aluminum alloy powders with 5%  $\text{Si}_3\text{N}_4$  reinforcement, processed for 30, 60, and 120 minutes of high-energy grinding. No significant changes were observed in the diffractograms across different milling times, indicating consistent high-energy milling processes

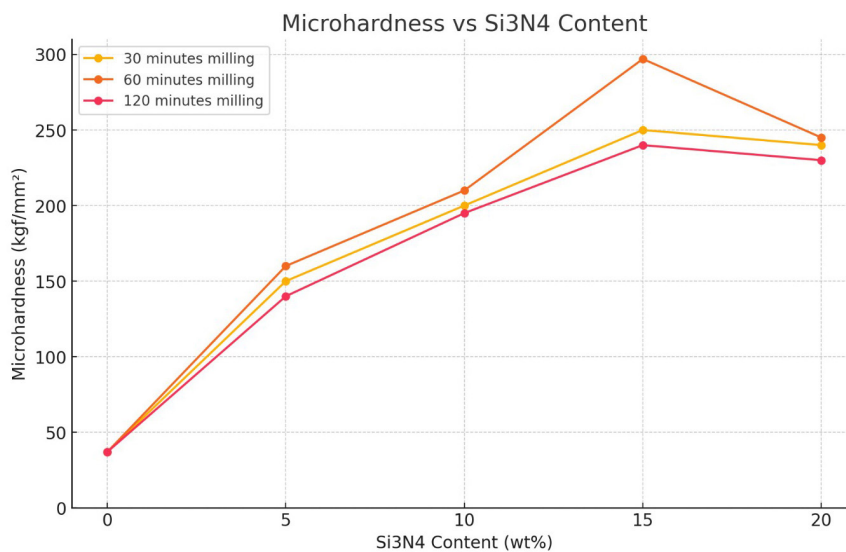


Figure 13: Microhardness Vs  $\text{Si}_3\text{N}_4$  Content.



and good homogeneity of the powders. The limited number of peaks is attributed to the minor fraction of  $\text{Si}_3\text{N}_4$  reinforcement (5%).

Similarly, Figures 15 and 16 present the diffractograms for AA 2124 powders with 10% and 15%  $\text{Si}_3\text{N}_4$  reinforcement, respectively, processed over the same durations. Although a higher quantity of  $\text{Si}_3\text{N}_4$  peaks was observed with increasing reinforcement, indicating better incorporation into the matrix, no significant changes in the diffractograms were noted for different milling times.

By comparing Figures 14, 15, and 16, an incremental increase in the number and magnitude of  $\text{Si}_3\text{N}_4$  peaks is evident with each increase in reinforcement. Figure 17, which depicts the diffractograms for 20%  $\text{Si}_3\text{N}_4$  reinforcement, further supports this observation, showing no significant changes across grinding times.

It was noted that the 30-minute grinding sessions resulted in the lowest peak intensities.

Figure 18, highlights the original, predominantly spherical morphology of the AA 2124 metal alloy powder received for the work, without reinforcement or undergoing high-energy grinding. This morphology is typical of ductile material and powder manufactured by the atomization method that promotes the solidification of the metal into finely divided particles.

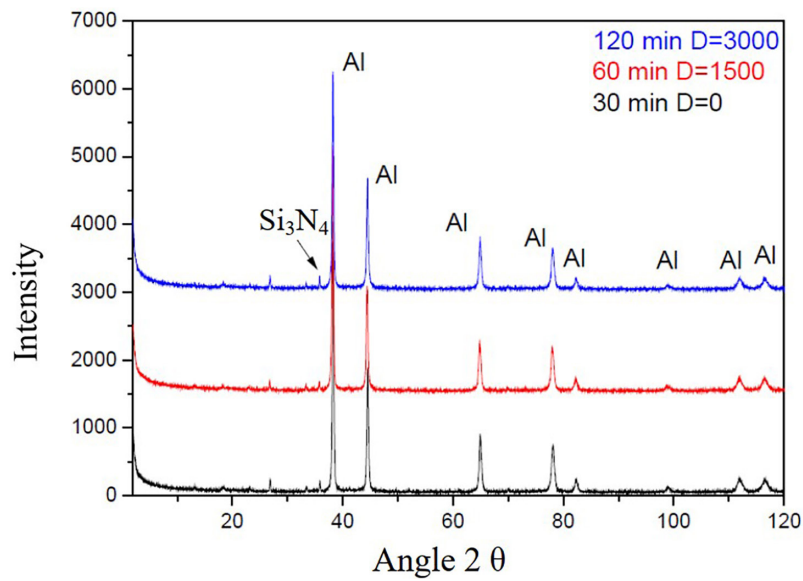


Figure 14: X-ray diffraction (XRD) result for AA 2124 + 5%  $\text{Si}_3\text{N}_4$  – 30, 60, 120 minutes MAE.

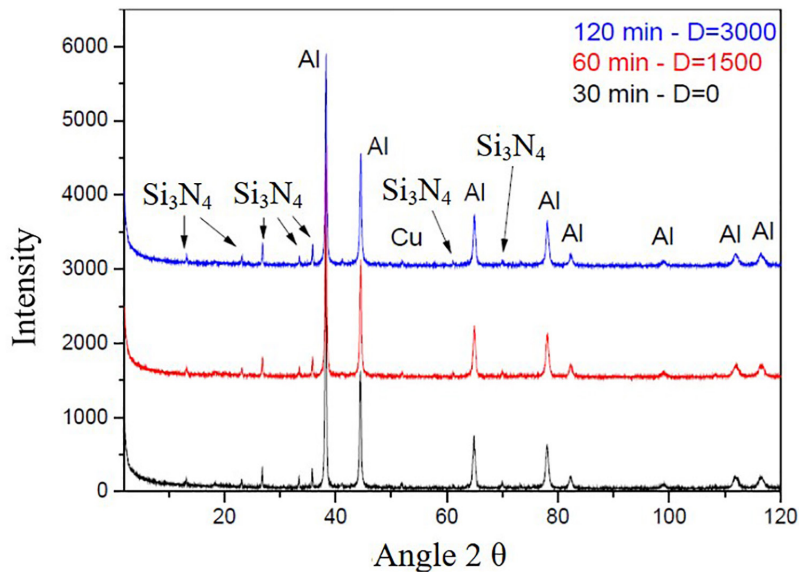


Figure 15: X-ray diffraction (XRD) results for AA 2124 + 10%  $\text{Si}_3\text{N}_4$  – 30, 60, 120 minutes MAE.



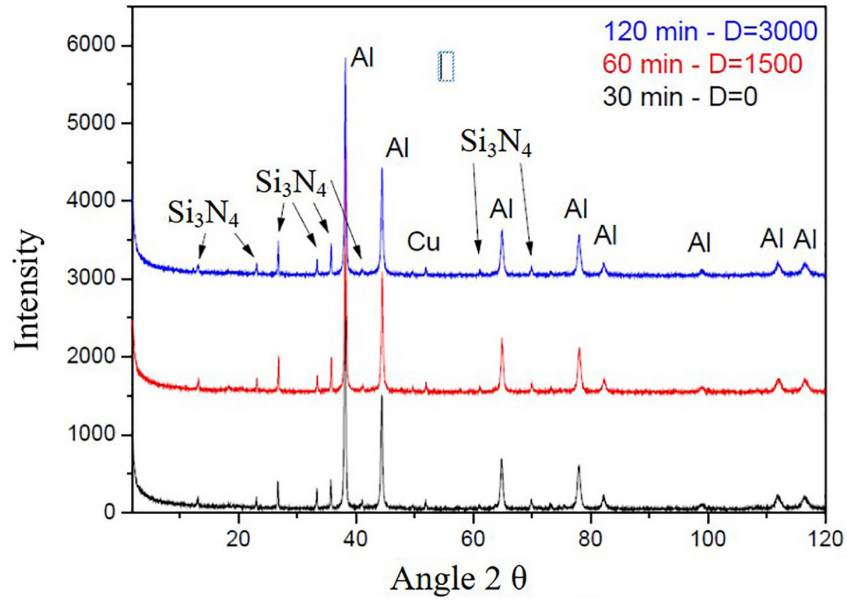


Figure 16: Result of X-ray diffraction (XRD) for AA 2124 + 15% Si<sub>3</sub>N<sub>4</sub> – 30, 60, 120 minutes MAE.

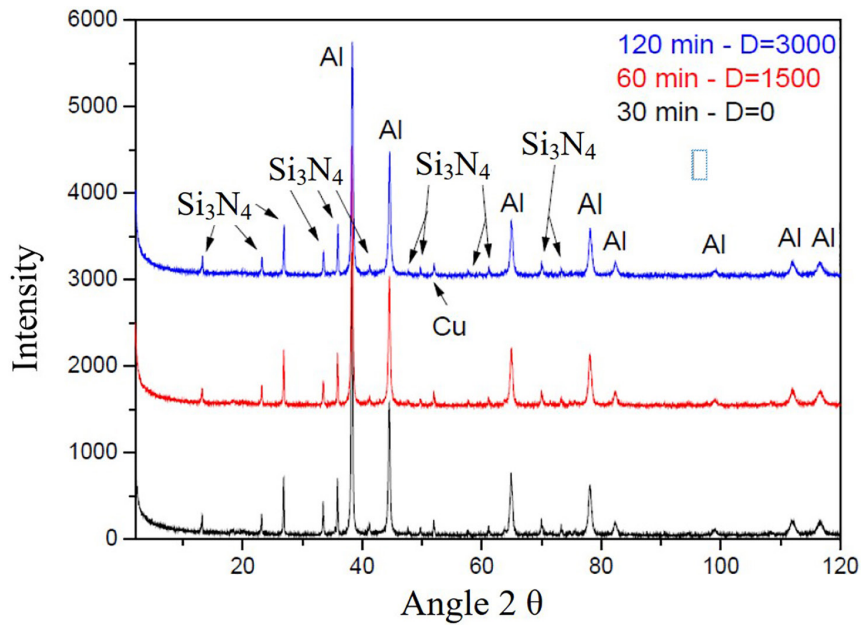


Figure 17: Result of X-ray diffraction (XRD) for AA 2124 + 20% Si<sub>3</sub>N<sub>4</sub> – 30, 60, 120 minutes MAE.

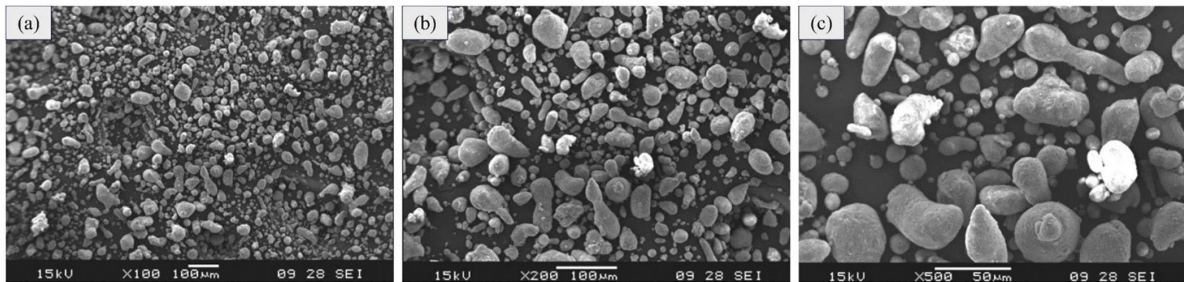


Figure 18: MEV AA 2124 100× (a), 200× (b) and 500× (c).

SEM and XRD thoroughly analyzed the interface between the AA2124 aluminum alloy matrix and  $\text{Si}_3\text{N}_4$  reinforcement. SEM micrographs revealed good interfacial integrity with minimal clustering of  $\text{Si}_3\text{N}_4$  particulates, ensuring efficient load transfer. XRD patterns confirmed the presence of  $\text{Si}_3\text{N}_4$  peaks without forming undesirable phases, indicating no significant chemical reactions occurred during processing. These findings suggest a stable interface conducive to enhanced mechanical properties. The MAE process modifies the AA 2124 alloy's originally spherical morphology to an equiaxial morphology, which is more conducive to the forming process, as it avoids the formation of directional properties.

Figure 19 shows the SEM analysis of a sample of AA 2124 aluminum alloy with 5%, 10%, 15%, and 20%  $\text{Si}_3\text{N}_4$  reinforcement at a grinding time of 30 min (MAE) at magnifications of 130 $\times$ , 250 $\times$ , 500 $\times$ , and 1000 $\times$ . The powders processed for 30 minutes showed morphology modified from originally spherical to more flattened and irregular morphologies. The particles were observed to be more deformed with 5%  $\text{Si}_3\text{N}_4$  reinforcement, where the powders weakened and presented fractures. Fractures are evident in Figures (c) and (d). The initial morphology of the powders is modified when the particles are subjected to continuous collisions of the balls, promoting repeated welds, fractures, and rewelds, allowing better microstructural control in the composite [44].

Figure 20 shows the SEM analysis of a sample of AA 2124 aluminum alloy with 5%, 10%, 15%, and 20%  $\text{Si}_3\text{N}_4$  reinforcement at a grinding time of 60 min (MAE) at magnifications of 130 $\times$ , 250 $\times$ , 500 $\times$ , and 1000 $\times$ . Using 60 minutes, modified as morphologies of the powders. Processed composites for 30 minutes, from flattened and irregular to morphologies closer to equiaxial, with morphologies tending to be spherical. It was observed that with the incorporation of 5%  $\text{Si}_3\text{N}_4$  reinforcement, the particles were more deformed where the powders weakened and presented fractures, and with increasing time, the particles became more deformed.

Figure 21 shows the SEM analysis of a sample of AA 2124 aluminum alloy with 5%, 10%, 15%, and 20%  $\text{Si}_3\text{N}_4$  reinforcement at a grinding time of 120 min (MAE) at magnifications of 130 $\times$ , 250 $\times$ , 500 $\times$ , and 1000 $\times$ . MAE modified the morphology of the processed composite with 30 minutes using 120 minutes. From close to equiaxial for a morphology with a pointed, brittle profile, similar to particles with dendritic morphology. The composites reinforced with 5%  $\text{Si}_3\text{N}_4$  and processed in MAE for 30 min revealed a coarser, flattened, and

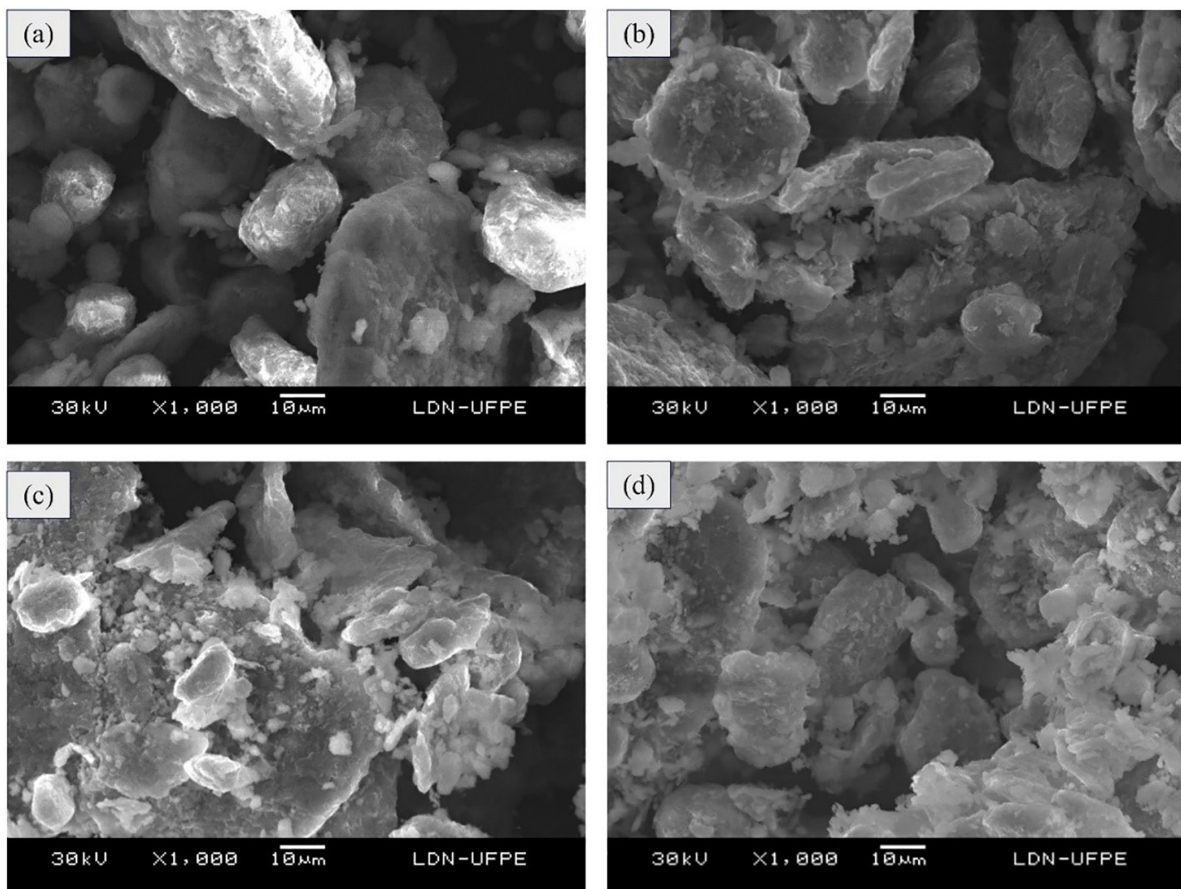


**Figure 19:** SEM AA 2124 + 5%, 10%, 15%, 20%  $\text{Si}_3\text{N}_4$  – 30 min MAE. – 5% (a), 10% (b), 15% (c), 20% (d).



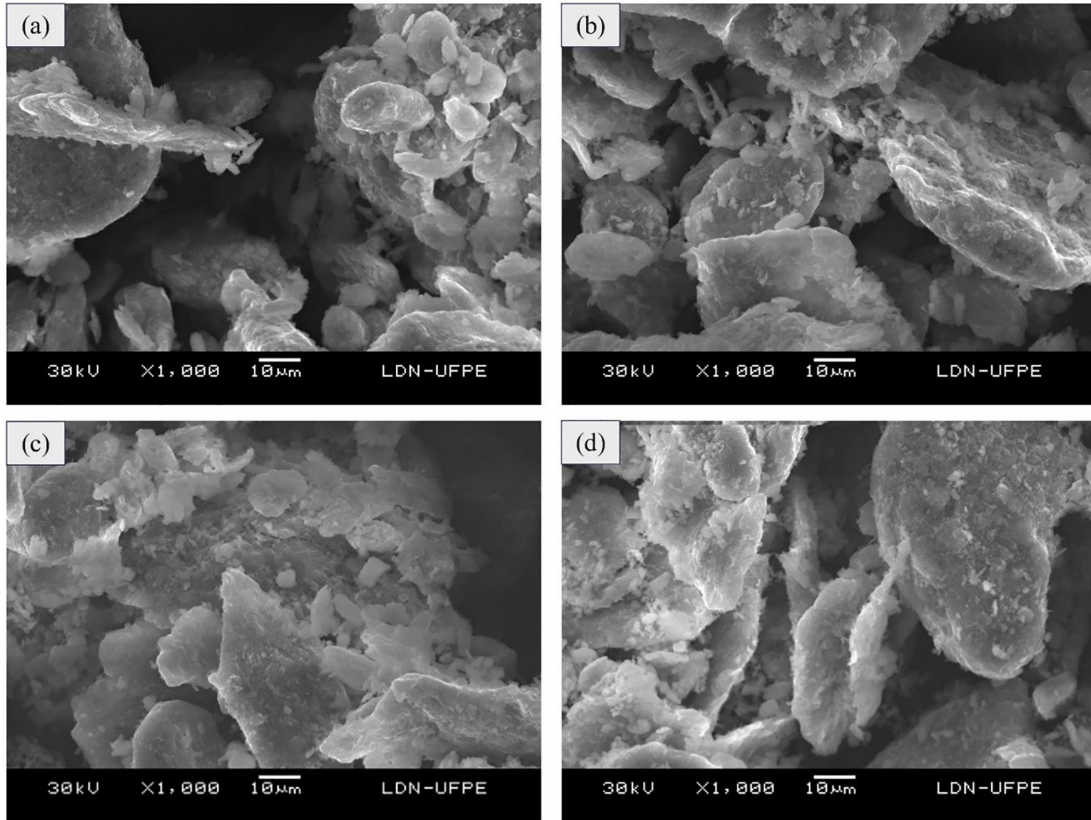


Figure 20: MEV AA 2124 + 5%, 10%, 15%, 20% Si<sub>3</sub>N<sub>4</sub> – 60 min MAE. – 5% (a), 10% (b), 15% (c), 20% (d).

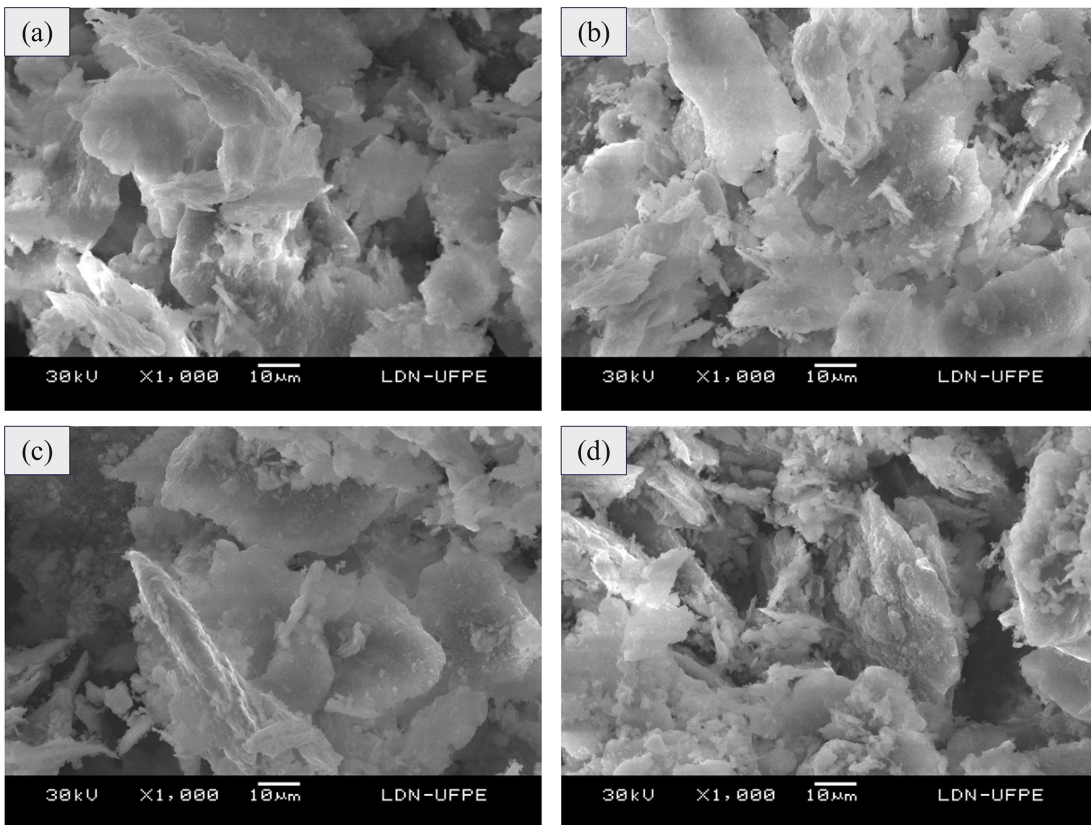


Figure 21: MEV AA 2124 + 5%, 10%, 15%, 20% Si<sub>3</sub>N<sub>4</sub> – 120 min MAE. – 5% (a), 10% (b), 15% (c), 20% (d).

irregular morphology. At the same time, with an increase in the grinding time to 120 minutes, we noticed the particles had a more refined morphology.

The potential for secondary processing of the developed composites, such as forming and machining, was assessed. The composites demonstrated good machinability with minimal tool wear and were amenable to forming processes such as extrusion and rolling. The enhanced mechanical properties and uniform distribution of Si<sub>3</sub>N<sub>4</sub> particulates contributed to the ease of secondary processing.

## 5. CONCLUSIONS

The outcomes establish correlations between processing conditions, microstructure parameters, and resulting mechanical properties, which can be applied to tailor the properties of the AA2124/Si<sub>3</sub>N<sub>4</sub> system for specific applications.

- High energy milling effectively distributes Si<sub>3</sub>N<sub>4</sub> particulate reinforcements in AA2124 aluminum alloy matrix with progressively reduced particle sizes at longer milling times. Powder morphologies transition from irregular to flattened lamellar and equiaxed structures on milling.
- Increasing Si<sub>3</sub>N<sub>4</sub> content from 5-20wt% results in progressively higher intensity Si<sub>3</sub>N<sub>4</sub> peaks in XRD analysis, corroborating the efficient incorporation of the reinforcement. No undesirable phases are formed, indicating compatibility of the Si<sub>3</sub>N<sub>4</sub> reinforcements.
- Sintered density increases from 93-94% for 5wt% Si<sub>3</sub>N<sub>4</sub> to 96-97% for 20wt% Si<sub>3</sub>N<sub>4</sub> due to improved particle packing. However, prolonged 120-minute milling causes greater porosity and lower density.
- Optical micrographs and SEM analysis confirm the uniform distribution of Si<sub>3</sub>N<sub>4</sub> particulates in the sub-micron size range of 2-3 μm for all composites. Minimal clustering is observed even at higher Si<sub>3</sub>N<sub>4</sub> levels.
- The microhardness increases with rising Si<sub>3</sub>N<sub>4</sub> content from 5-15wt% due to the strengthening effect of the nanosized ceramic particulates as obstacles to dislocation motion. Excessive addition of 20wt% Si<sub>3</sub>N<sub>4</sub> leads to particle clustering and a fall in hardness.
- Among milling times, 60 minutes is optimal, with the highest composite hardness due to the appropriate balance between work hardening and particle fracturing. Lower and higher times show inferior properties.

The uniform distribution of Si<sub>3</sub>N<sub>4</sub> nanoparticles, good interfacial integrity, and enhanced hardness validate the potential of powder metallurgy synthesis combined with optimized high-energy ball milling for developing high-performance aluminum alloy-based metal matrix nanocomposites.

## 6. BIBLIOGRAPHY

- [1] AKBARPOUR, M.R., GAZANI, F., MOUSA MIRABAD, H., *et al.*, “Recent advances in processing, and mechanical, thermal and electrical properties of Cu-SiC metal matrix composites prepared by powder metallurgy”, *Progress in Materials Science*, v. 140, pp. 140, 2023. doi: <http://doi.org/10.1016/j.pmatsci.2023.101191>.
- [2] BROSLER, P., SILVA, R.F., TEDIM, J., *et al.*, “Electroconductive silicon nitride-titanium nitride ceramic substrates for CVD diamond electrode deposition”, *Ceramics International*, v. 49, n. 22, pp. 36436–36445, 2023. doi: <http://doi.org/10.1016/j.ceramint.2023.08.327>.
- [3] CHAUDHARY, B., PATEL, M., JAIN, N.K., *et al.*, “Friction stir powder additive manufacturing of Al 6061/FeCoNi and Al 6061/Ni metal matrix composites: reinforcement distribution, microstructure, residual stresses, and mechanical properties”, *Journal of Materials Processing Technology*, v. 319, pp. 319, 2023. doi: <http://doi.org/10.1016/j.jmatprotec.2023.118061>.
- [4] CHEN, D., LI, J., SUN, K., *et al.*, “Graphene-reinforced metal matrix composites: fabrication, properties, and challenges”, *International Journal of Advanced Manufacturing Technology*, v. 125, n. 7-8, pp. 2925–2965, 2023. doi: <http://doi.org/10.1007/s00170-023-10886-4>.
- [5] DWIVEDI, S.P., SHARMA, S., MISHRA, R.K., “Characterization of waste eggshells and CaCO<sub>3</sub> reinforced AA2014 green metal matrix composites: a green approach in the synthesis of composites”, *International Journal of Precision Engineering and Manufacturing*, v. 17, n. 10, pp. 1383–1393, 2016. doi: <http://doi.org/10.1007/s12541-016-0164-z>.
- [6] FERNÁNDEZ, H., ORDOÑEZ, S., PESENTI, H., *et al.*, “Microstructure homogeneity of milled aluminum A356-Si<sub>3</sub>N<sub>4</sub> metal matrix composite powders”, *Journal of Materials Research and Technology*, v. 8, n. 3, pp. 2969–2977, 2019. doi: <http://doi.org/10.1016/j.jmrt.2019.05.004>.

- [7] GAWDZIŃSKA, K., CHYBOWSKI, L., PRZETAKIEWICZ, W., “Proper matrix-reinforcement bonding in cast metal matrix composites as a factor of their good quality”, *Archives of Civil and Mechanical Engineering*, v. 16, n. 3, pp. 553–563, 2016. doi: <http://doi.org/10.1016/j.acme.2015.11.004>.
- [8] GUAN, D., HE, X., ZHANG, R., *et al.*, “Microstructure and tensile properties of in situ polymer-derived particles reinforced steel matrix composites produced by powder metallurgy method”, *Materials Science and Engineering A*, v. 705, pp. 231–238, 2017. doi: <http://doi.org/10.1016/j.msea.2017.07.084>.
- [9] IVANOV, O.N., YAPRYNTSEV, M.N., Vasil’ev, A.E., *et al.*, “Microstructure features of metal-matrix composites based on thermoelectric bismuth telluride matrix and ferromagnetic filler”, *Glass and Ceramics*, v. 78, n. 11–12, pp. 442–447, 2022. doi: <http://doi.org/10.1007/s10717-022-00428-x>.
- [10] JAYALAKSHMI, S., SINGH, R.A., CHEN, X., *et al.*, “Role of matrix microstructure in governing the mechanical behavior and corrosion response of two magnesium alloy metal matrix composites”, *Journal of the Minerals Metals & Materials Society*, v. 72, n. 8, pp. 2882–2891, 2020. doi: <http://doi.org/10.1007/s11837-020-04166-9>.
- [11] KIM, C.S., CHO, K., MANJILI, M.H., *et al.*, “Mechanical performance of particulate-reinforced Al metal-matrix composites (MMCs) and Al metal-matrix nano-composites (MMNCs)”, *Journal of Materials Science*, v. 52, n. 23, pp. 13319–13349, 2017. doi: <http://doi.org/10.1007/s10853-017-1378-x>.
- [12] KOCAMAN, M., AKÇAY, S.B., GÜLER, O., *et al.*, “The effect of recycled zinc powder content on the properties of novel novolac matrix hybrid composites”, *Tribology International*, v. 188, pp. 188, 2023. doi: <http://doi.org/10.1016/j.triboint.2023.108814>.
- [13] KRYAZHEV, Y.G., ANIKEEVA, I.V., TRENKIN, M.V., *et al.*, “Synthesis of metal-carbon composites with transition metal nanoparticles distributed as metal core-graphite-like shell structures in the bulk of an amorphous carbon matrix”, *Solid Fuel Chemistry*, v. 53, n. 5, pp. 289–293, 2019. doi: <http://doi.org/10.3103/S0361521919050069>.
- [14] KUMAR, D., SEETHARAM, R., PONAPPA, K., “A review on microstructures, mechanical properties and processing of high entropy alloys reinforced composite materials”, *Journal of Alloys and Compounds*, v. 972, pp. 972, 2024. doi: <http://doi.org/10.1016/j.jallcom.2023.172732>.
- [15] LI, J., NI, J., HUANG, B., *et al.*, “Long-term ball milling and hot pressing of in-situ nanoscale tungsten carbides reinforced copper composite and its characterization”, *Materials Characterization*, v. 152, pp. 134–140, 2019. doi: <http://doi.org/10.1016/j.matchar.2019.04.014>.
- [16] LIAO, Z., HUANG, X., ZHANG, F., *et al.*, “Effect of WC mass fraction on the microstructure and frictional wear properties of WC/Fe matrix composites”, *International Journal of Refractory & Hard Metals*, v. 114, pp. 114, 2023. doi: <http://doi.org/10.1016/j.ijrmhm.2023.106265>.
- [17] LOGESH, G., LODHE, M., BALASUBRAMANIAN, M., “Effect of temperature and gaseous medium on the evolved microstructures of carbon fiber reinforced reaction bonded silicon nitride composites”, *Ceramics International*, v. 43, n. 8, pp. 6110–6116, 2017. doi: <http://doi.org/10.1016/j.ceramint.2017.02.004>.
- [18] MENG, Q., CHEN, C., ARABY, S., *et al.*, “Highly ductile and mechanically strong Al-alloy/boron nitride nanosheet composites manufactured by laser additive manufacturing”, *Journal of Manufacturing Processes*, v. 89, pp. 384–396, 2023. doi: <http://doi.org/10.1016/j.jmapro.2023.01.051>.
- [19] MUKHAMETRAKHIMOV, M.K., “Titanium-alloy metal matrix composites produced by low-temperature superplastic pressure welding”, *Russian Engineering Research*, v. 41, n. 4, pp. 315–319, 2021. doi: <http://doi.org/10.3103/S1068798X21040171>.
- [20] PARIKH, V.K., PATEL, V., PANDYA, D.P., *et al.*, “Current status on manufacturing routes to produce metal matrix composites: state-of-the-art”, *Heliyon*, v. 9, n. 2, pp. 9, 2023. doi: <http://doi.org/10.1016/j.heliyon.2023.e13558>. PubMed PMID: 36846686.
- [21] PEZESHKIAN, M., EBRAHIMZADEH, I., “Investigating the role of metal reinforcement particles in producing Cu/Ni/W metal matrix composites via friction stir processing: microstructure, microhardness, and wear at high temperature”, *Metals and Materials International*, 2023. doi: <http://doi.org/10.1007/s12540-023-01488-6>.
- [22] SADHU, K.K., MANDAL, N., SAHOO, R.R., “SiC/graphene reinforced aluminum metal matrix composites prepared by powder metallurgy: a review”, *Journal of Manufacturing Processes*, v. 91, pp. 10–43, 2023. doi: <http://doi.org/10.1016/j.jmapro.2023.02.026>.
- [23] SHEINERMAN, A.G., “Mechanical properties of metal matrix composites with graphene and carbon nanotubes”, *The Physics of Metals and Metallography*, v. 123, n. 1, pp. 57–84, 2022. doi: <http://doi.org/10.1134/S0031918X22010124>.

- [24] SONG, J., LIU, Y., MEI, S., *et al.*, “Purifying metallurgical-grade silicon to 4N with 3D porous structure by integrated metallurgy-materials phase separation”, *Chemical Engineering Journal*, v. 454, pp. 454, 2023. doi: <http://doi.org/10.1016/j.cej.2022.140092>.
- [25] TOOZANDEHJANI, M., OSTOVAN, F., JAMALUDIN, K.R., *et al.*, “Process– microstructure– properties relationship in Al– CNTs– Al<sub>2</sub>O<sub>3</sub> nanocomposites manufactured by hybrid powder metallurgy and microwave sintering process”, *Transactions of Nonferrous Metals Society of China*, v. 30, n. 9, pp. 2339–2354, 2020. doi: [http://doi.org/10.1016/S1003-6326\(20\)65383-3](http://doi.org/10.1016/S1003-6326(20)65383-3).
- [26] VOROZHTSOV, S., KOLARIK, V., PROMAKHOV, V., *et al.*, “The influence of Al<sub>4</sub>C<sub>3</sub> nanoparticles on the physical and mechanical properties of metal matrix composites at high temperatures”, *Journal of the Minerals Metals & Materials Society*, v. 68, n. 5, pp. 1312–1316, 2016. doi: <http://doi.org/10.1007/s11837-016-1854-9>.
- [27] WANG, Y., ZHU, Y., LI, R., *et al.*, “High-performance aluminum-based matrix composites reinforced with high content of boron nitride nanosheets”, *Journal of Alloys and Compounds*, v. 906, pp. 164358, 2022. doi: <http://doi.org/10.1016/j.jallcom.2022.164358>.
- [28] XU, T., ZHU, Z., MI, G., *et al.*, “Silicon nitride assisted carbon nanotubes induced stacking faults and twins in aluminum alloy composite joint”, *Journal of Materials Research and Technology*, v. 25, pp. 6965–6976, 2023. doi: <http://doi.org/10.1016/j.jmrt.2023.07.148>.
- [29] YÖNETKEN, A., “Fabrication of electroless Ni plated Fe-Al<sub>2</sub>O<sub>3</sub> ceramic-metal matrix composites”, *Transactions of the Indian Institute of Metals*, v. 68, n. 5, pp. 675–681, 2015. doi: <http://doi.org/10.1007/s12666-014-0497-1>.
- [30] ZHANG, R., LI, W., ZHANG, X., *et al.*, “Modeling the temperature-dependent Young’s modulus of short fiber reinforced metal matrix composites and its particle hybrid composites”, *International Journal of Mechanics and Materials in Design*, v. 18, n. 4, pp. 837–851, 2022. doi: <http://doi.org/10.1007/s10999-022-09611-y>.
- [31] ABUSHANAB, W.S., MOUSTAFA, E.B., GHANDOURAH, E.I., *et al.*, “Impact of hard and soft reinforcements on the microstructure, mechanical, and physical properties of the surface composite matrix manufactured by friction stir processing”, *Coatings*, v. 13, n. 2, pp. 284, 2023. doi: <http://doi.org/10.3390/coatings13020284>.
- [32] ABUSHANAB, W.S., MOUSTAFA, E.B., GHANDOURAH, E., *et al.*, “The effect of different fly ash and vanadium carbide contents on the various properties of hypereutectic Al-Si alloys-based hybrid nanocomposites.”, *Silicon*, v. 14, n. 10, pp. 5367–5377, 2022. doi: <http://doi.org/10.1007/s12633-021-01284-0>.
- [33] ABUSHANAB, W.S., MOUSTAFA, E.B., GODA, E.S., *et al.*, “Influence of vanadium and niobium carbide particles on the mechanical, microstructural, and physical properties of AA6061 aluminum-based mono-and hybrid composite using FSP”, *Coatings*, v. 13, n. 1, pp. 142, 2023. doi: <http://doi.org/10.3390/coatings13010142>.
- [34] EL-ZAIDIA, M.M., ZAKI, M.Z., ABOMOSTAFA, H.M., *et al.*, “Comprehensive studies for evaluating promising properties of Cu/graphene/fly ash nanocomposites”, *Scientific Reports*, v. 14, n. 1, pp. 2236, 2024. <http://doi.org/10.1038/s41598-024-52563-w>. PubMed PMID: 38278959.
- [35] ISSA, S.A.M., ALMUTAIRI, A.M., ALBALAWI, K., *et al.*, “Production of hybrid nanocomposites based on iron waste reinforced with niobium carbide/granite nanoparticles with outstanding strength and wear resistance for use in industrial applications”, *Nanomaterials (Basel, Switzerland)*, v. 13, n. 3, pp. 537, 2023. doi: <http://doi.org/10.3390/nano13030537>. PubMed PMID: 36770498.
- [36] MOUSTAFA, E.B., ABDEL AZIZ, S.S., TAHA, M.A., *et al.*, “Influence of graphene and silver addition on aluminum’s thermal conductivity and mechanical properties produced by the powder metallurgy technique”, *Metals*, v. 13, n. 5, pp. 836, 2023. doi: <http://doi.org/10.3390/met13050836>.
- [37] KHOSHAIM, A.B., MOUSTAFA, E.B., ALAZWARI, M.A., *et al.*, “An investigation of the mechanical, thermal and electrical properties of an AA7075 alloy reinforced with hybrid ceramic nanoparticles using friction stir processing”, *Metals*, v. 13, n. 1, pp. 124, 2023. doi: <http://doi.org/10.3390/met13010124>.
- [38] MOUSTAFA, E.B., ABUSHANAB, W.S., GHANDOURAH, E.I., *et al.*, “Advancements in surface reinforcement of AA2024 alloy using hybridized niobium carbide and ceramics particles via FSP technique”, *Metals and Materials International*, v. 30, n. 3, pp. 800–813, 2024. doi: <http://doi.org/10.1007/s12540-023-01541-4>.

- [39] MOUSTAFA, E.B., ALJABRI, A., ABUSHANAB, W.S., *et al.*, “A comprehensive study of Al-Cu-Mg system reinforced with nano-ZrO<sub>2</sub> particles synthesized by powder metallurgy technique”, *Scientific Reports*, v. 14, n. 1, pp. 2862, 2024. doi: <http://doi.org/10.1038/s41598-024-53061-9>. PubMed PMID: 38311645.
- [40] MOUSTAFA, E.B., ELSHEIKH, A.H., TAHA, M.A., “The effect of TaC and NbC hybrid and mono-nanoparticles on AA2024 nanocomposites: microstructure, strengthening, and artificial aging”, *Nanotechnology Reviews*, v. 11, n. 1, pp. 2513–2525, 2022. doi: <http://doi.org/10.1515/ntrev-2022-0144>.
- [41] TAHA, M.A., EL-ZAIDIA, M.M., ZAKI, M.Z., *et al.*, “Influence of nano-hybrid reinforcements on the improvement strength, thermal expansion and wear properties of Cu-SiC-Fly ash nanocomposites prepared by powder metallurgy”, *ECS Journal of Solid State Science and Technology: JSS*, v. 12, n. 3, pp. 033011, 2023. doi: <http://doi.org/10.1149/2162-8777/acc5af>.
- [42] MANHÃES, W.S., SILVA, L.R.R.D., ZANCANELLA, A.C.B., *et al.*, “Metallographic and mechanical characterization of ABNT/SAE 1020 steel subjected to the thermochemical treatment of carburizing and the thermal treatment of the quenching”, *Matéria (Rio de Janeiro)*, v. 27, pp. e13228, 2023.
- [43] GNANIAH, A.M., SEHAR, F.I.R.E., MANGALARAJ, A., *et al.*, “Thermal analysis of modified segmented switched reluctance motor with aluminium metal matrix composite fins used in cooling fan applications”, *Matéria (Rio de Janeiro)*, v. 29, n. 2, pp. e20240075, 2024. doi: <http://doi.org/10.1590/1517-7076-rmat-2024-0075>.
- [44] RAMADAN, S., TAHA, M.A., EL-MELIGY, W.M., *et al.*, “Influence of graphene content on sinterability and physico-mechanical characteristics of Al/Graphene Composites Prepared via”, *Biointerface Research in Applied Chemistry*, v. 13, n. 2, pp. 192, 2022. doi: <http://doi.org/10.33263/BRIAC132.192>.